Comment from the editor:

Dear Authors,

Thank you for addressing my comments at this stage. I will go ahead and start the formal review process (ACPD). I did want to point out that your Figure 1 in the reply has a mass spectrum similar to Figure 1 from Hatch et al. (2011, ES&T). Hatch et al. saw a small fraction as well, but is this due to the ionization efficiency being low? Meaning, even though the ion intensity is low, do you really know if that means it is low in abundance in the RES? Please consider that comment during the review process.

Thanks for your handling and comments to further improve our manuscript. It is possible that the ionization efficiency may lead to the small fraction of organosulfate, however, there is still no data to support this. Thus, we cannot confirm that it is low in abundance in the RES, since the SPAMS only provides the relative intensity of ion peaks, which can be used to indicate the relative abundance of a species in a particle. However, we observed both the small number fraction of particles containing organosulfate and extremely low relative intensity for organosulfate may still reflect the limited occurrence of organosulfate in the RES.

Comment from Referee #1:

Interactive comment on "Impact of in-cloud aqueous processes on the chemical compositions and morphology of individual atmospheric aerosols" by Yuzhen Fu et al. Anonymous Referee #1 Received and published: 26 May 2020

In this paper, the authors did a good job of presenting their results on the different morphologies and mixing states of activated and interstitial particles. I think that the analysis could be strengthened by further exploring the connection between the offline TEM-EDS analysis and the online SPAMS analysis.

We would like to thank the referee for the positive and valuable comments to improve our manuscript. We agree with the comments and have strengthened the analysis, in particular, the connection between the TEM/EDS and the SPAMS results. As suggested, the size distribution and mass spectral information were included to support the discussion. We have addressed the specific comments in the sections below and made the appropriate revisions to the manuscript. The referee's comments are in the black text followed by our response in the blue text.

As Prof. Surratt mentioned, it has been previously shown that SOA can form via in-cloud processes and the formation of SOA can result in core-shell phase morphology. As such, it would be beneficial to assess the SPAMS mass spectra for SOA products, especially given the increase in the number fraction of S-OM relative to S-rich particles in the RES v. INT particles.

Thanks for your comment. Indeed, we also hope to obtain more information about OM from SPAMS to explain and corroborate the results obtained from TEM/EDS. In the section 3.3, we use the ratios of relative peak area of organics to sulfate of OM particles during in-cloud (RES and INT) and pre-cloud (Ambient) periods from the data of SPAMS (Table S2), to help explain the in-cloud formation of OM found by TEM/EDS, which show that the ratios of relative peak area between organics and sulfate are similar

Additionally, the size distribution of different particle morphologies and mixing states could be assessed and compared to the size-resolved mass spectra from the SPAMS.

The size distribution of different particle types revealed that S-rich and aged soot particles were predominant in smaller size segments, and aged mixture particles in larger size segments (Figure S8). Likewise, the size-resolved number fractions of different particle types from the results of the SPAMS also showed that the BC-containing particles were mainly distributed between 0.1 and 1.3 µm, representing ~80% of the submicron RES and ~73% of the submicron INT population, respectively (Figure S9).
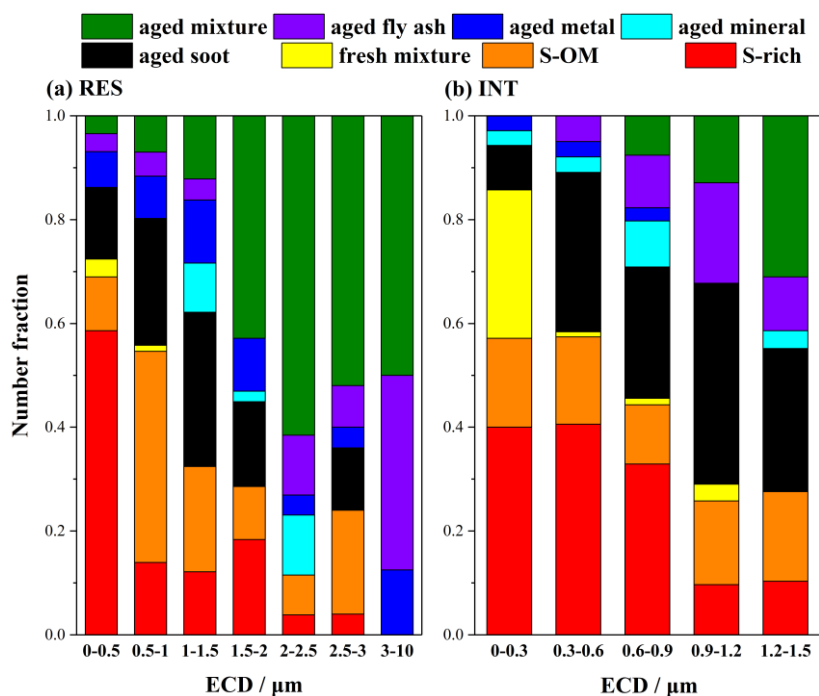
Figure S8. Size-resolved number fraction distributions of RES and INT by TEM/EDS.
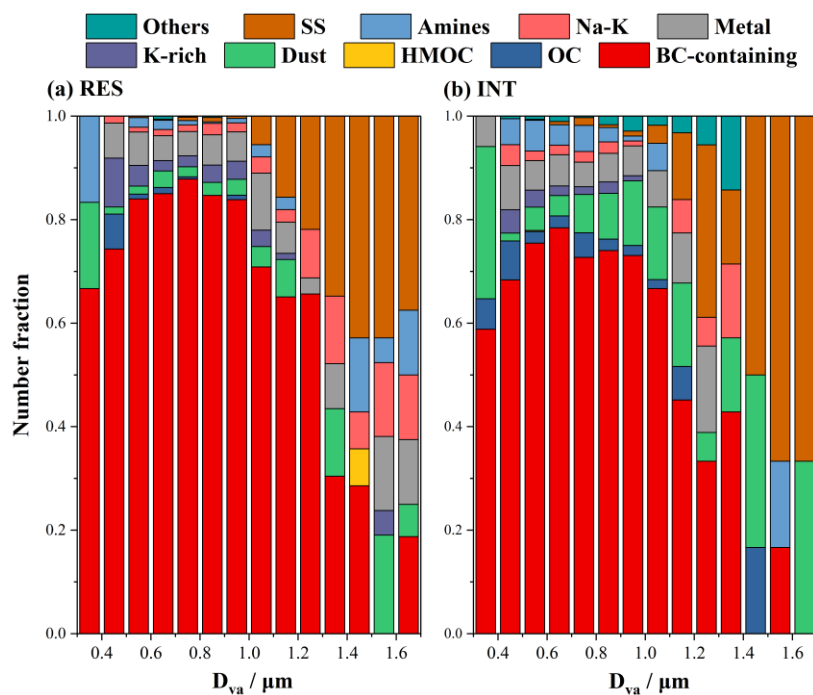
Figure S9. Size-resolved number fraction distributions of RES and INT by SPAMS.

Additionally, I would recommend that the authors include the EDS spectra that correspond to the TEM images presented in Figure 3.

Thanks for your suggestion. We have added the EDS spectra of the OM-containing particles corresponding to each TEM image in Figure 3 (that is Figure 5 now):
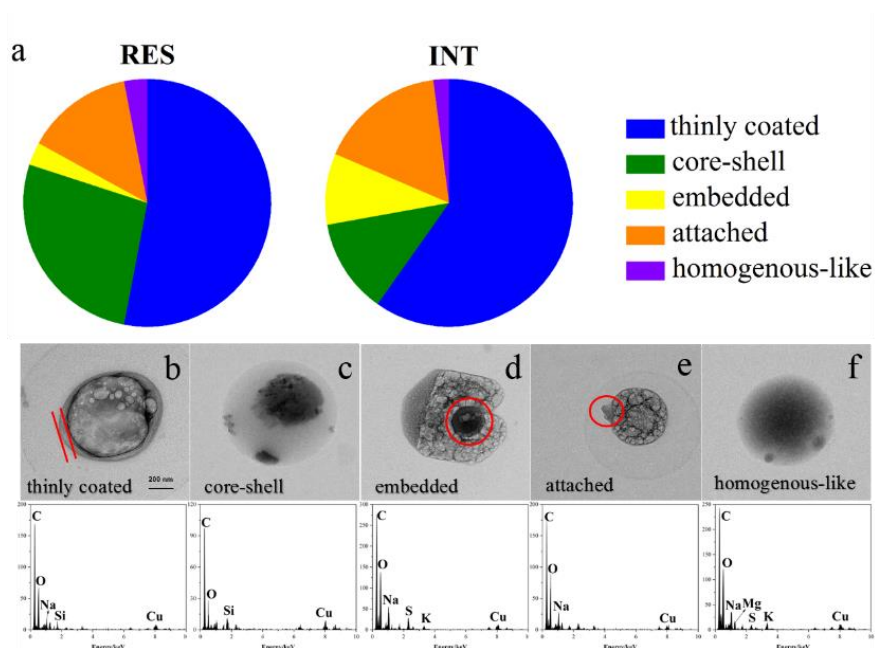
Figure 5. Number fractions of the OM-containing particles with different mixing structures in the RES and INT (a) and typical TEM images and corresponding EDS spectra of OM: thinly coated (b); core-shell (c); embedded (d); attached (e); homogenous-like (f) during cloud event #2 and #3.

In the SI, to clarify the difference between figures S1 and S3, I would recommend that the authors change the title of S1 to indicate that the fraction types correspond to EDS.

Thanks for pointing out this. We have changed the title of Figure S1 (that is Figure 3 now) from "Number fraction of different particle types in the RES during three cloud events." to "Number fraction of different particle types in the RES during three cloud events measured by TEM/EDS.".

Comment from Referee #2:

General:

This paper compares single-particle measurements of particle size, composition, and morphology of in-cloud and interstitial particles collected at a rural site in China. This paper mainly comments on the role of aqueous chemistry in forming organic shells and the observation of more branched soot particles in cloud. I have several comments about this work to be considered before publication.

We appreciate the constructive suggestions and comments from the referee. The referee's comments are in the black text followed by our response in the blue text as follows.

Major Comments:

1. A lot of the most important details and figures are in the SI rather than in the main text. Also, a lot of the main supporting data came from SPAMS analysis which was not described in the methods.

Thanks for your suggestions. We have moved some tables and figures from the SI to the main text, and we have added more information about the SPAMS in the methods. Please see below for specific responses.

2. The argument regarding core-shell and liquid-liquid phase separations was a bit confusing since previous work has shown that the core-shell morphology can break down as RH is increased.

We agree with your comment. What we want to express is that the oxidized organic matter formed in the cloud processes has a great influence on the mixing structure of organic particles after water evaporation within particles, which is conducive to the existence of organic particles in a core-shell structure after cloud events. Since we did not express clearly, we modified the relevant statements in the manuscript. Please refer

to lines 36-37 and 319-322:

Lines 36-37: The sentence, "Our results highlight the in-cloud formation of more oxidized organic shells on the activated particles.", has been changed to "Our results highlight that the formation of more oxidized organic matter in the cloud contributes to the existence of organic shells after cloud processing.".

Lines 319-322: The sentence, "The prevalence of OM shelled particles upon in-cloud processes also supports a recent laboratory observation depicting that rapid film formation and fast heterogeneous oxidation can provide an efficient way of converting water-insoluble organic films into more water-soluble components in aerosols or cloud droplets (Aumann and Tabazadeh, 2008).", has been changed to "The prevalence of OM shelled particles after cloud processing also supports a current laboratory observation depicting that rapid film formation and fast heterogeneous oxidation can provide an efficient way of converting water-insoluble organic films into more water-soluble components in aerosols or cloud droplets (Aumann and Tabazadeh, 2008).".

Specific Comments:

Introduction:

1. Lines 59-60: Nitric oxide is a gas, not particulate matter.

Thank you for pointing out this. In the article we quoted, the authors used "nitric oxide" to represent the NO^+ signal measured by ATOFMS, which refers to nitrate. In order to avoid ambiguity, we have changed "nitric oxide" to "nitrate".

2. Line 63: not sure how "decomposed" is being used in this sentence.

We are sorry for the misunderstanding. The word (decomposed) has been removed, and the sentence has been changed to "These results indicate that both RES and INT present complex mixtures, and carbonaceous matter (i.e., organic materials (OM) and soot) is important material in the cloud mass.". Please refer to lines 62-63.

3. Line 76: reword "this process might not be neglected"

The sentence, "this process might not be neglected.", has been changed to "the influence of this process in atmospheric chemistry cannot be neglected.". Please refer to lines 75-76.

4. Line 78: Also see [Moffet and Prather, 2009]

The literature has been cited in the main text. Please refer to lines 77-79:
"For another type of carbonaceous material, soot, there is extensive evidence that the absorption and cloud activation of soot-containing particles can be significantly affected by coatings (Adachi et al., 2010; Wu et al., 2018; Moffet and Prather, 2009)."

5. Lines 77-86: please also comment on the finding that organic coatings caused the collapse of soot particles from [Spencer and Prather, 2006].

The original sentence, "While some studies have found that soot compaction occurs after cloud processing (Bhandari et al., 2019; Ma et al., 2013; Mikhailov et al., 2006), Khalizov et al. (2013) suggested that soot with thin organic coating did not become more compact under high humidity.", has been changed to "While some studies have found that soot restructuring occurs after water processing (Bhandari et al., 2019; Ma et al., 2013; Mikhailov et al., 2006), or being coated by OM (Spencer and Prather, 2006) and sulfate (Zhang et al., 2008), Khalizov et al. (2013) suggested that soot with thin organic coating did not become more compact under high humidity." Please refer to lines 83-86.

Reference:
Spencer, M. T., and Prather, K. A.: Using ATOFMS to determine OC/EC mass fractions in particles, Aerosol Science and Technology, 40, 585-594,

10.1080/02786820600729138, 2006.

Zhang, R., Khalizov, A. F., Pagels, J., Zhang, D., Xue, H., and McMurry, P. H.: Variability in morphology, hygroscopicity, and optical properties of soot aerosols during atmospheric processing, Proceedings of the National Academy of Sciences of the United States of America, 105, 10291-10296, 10.1073/pnas.0804860105, 2008.

Methods:

1. Lines 100-101: What is meant by "almost unaffected by local anthropogenic sources"?

The sampling site is surrounded by a national park forest (273 km^2), and there are scarcely any emissions from anthropogenic activities.

2. Lines 117-120: I think that Table S1 and the air mass back trajectories should be shown in the main paper. It will help give context for what was different between the different cloud events to help interpret the results.

We agree with you. Table S1 and Figure S2 (the air mass back trajectories) have been moved to the main text, and are numbered as Table 1 and Figure 4.

3. Line 125: change "folds" to "fold".

It has been changed accordingly.

4. Line 128: change "vacuumed" to "vacuum" and define NH$_4$NO$_3$.

It has been changed accordingly. The sentence has been changed to "In the TEM vacuum chamber, some volatile substances (e.g., ammonium nitrate (NH$_4$NO$_3$) and volatile organic matter) would be lost.". Please refer to lines 129-130.

5. I couldn't follow the methodology given in section 2.4. Please add more details.

9

We have added detailed calculations in the section 2.4 (that is section 2.5 now). We have now included an introduction on two parameters including k_a and α, which depends on the degree of monomer overlap (δ) in the aggregate. Furthermore, we have also supplemented the calculation of δ herein. Please refer to lines 174-180:

"The value of k_a and α depends on the degree of monomer overlap (δ) in the aggregate (Oh and Sorensen, 1997), and δ can be determined by:

$$\delta = \frac{2a}{l}$$

where a is monomer radius, and l is the center distance of adjacent monomers. The value of parameters including a, l, A_a, A_p, L_{max}, and d_p can be obtained by analyzing TEM images. Then D_f can be calculated by the above four formulas."

Reference:

Oh, C., and Sorensen, C. M.: The effect of overlap between monomers on the determination of fractal cluster morphology, Journal of Colloid and Interface Science, 193, 17-25, 10.1006/jcis.1997.5046, 1997.

6. A lot of SPAMS data is brought in to corroborate the results. I suggest that details on the SPAMS needs to be added to the methods if the data is being used.

The detailed information of the SPAMS has been added in the methods (section 2.4). And the identification of particles measured by the SPAMS is provided in the SI.

Results:

1. Line 153: some fresh soot particles can have sulfate, see [Moffet and Prather, 2009].

We agree with your comment. Since there is hardly any anthropogenic source around our sampling site, the collected soot particles are assumed to experience long-distance

transport and complex aging processes. The aging state of the soot particles may also be reflected by the associated more intense sulfate peaks measured by the SPAMS, compared with those observed in urban areas, as discussed in our previous publication (Zhang et al., 2017). Considering that much secondary inorganic matter and organic matter might be generated during the cloud processes, this study distinguishes fresh and aged particles by the presence or absence of secondary inorganic matter (S-rich) and organic matter (OM).

Zhang, G., Lin, Q., Peng, L., Bi, X., Chen, D., Li, M., Li, L., Brechtel, F. J., Chen, J., Yan, W., Wang, X., Peng, P., Sheng, G., and Zhou, Z.: The single-particle mixing state and cloud scavenging of black carbon: a case study at a high-altitude mountain site in southern China, Atmospheric Chemistry and Physics, 17, 14975-14985, 10.5194/acp-17-14975-2017, 2017.

2. Lines 154-156: the methods for identifying each component should be moved from the SI to the methods section of the paper.

The identification of each component has been moved from SI to the methods section of main text (section 2.3), and original sentence of lines 154-156, "The details involving the identification of each component (S, OM, soot, mineral, metal, fly ash) are provided in the Supporting Information.", has been canceled.

3. Lines 159-161: I would think it would be important to explicitly detail the mixture for your results. I found these classifications really confusing and hard to keep straight.

Thanks for your comment. Fresh mixture has been changed to "refractory" in the full text and SI, and the sentence has been changed to "Aged particle types containing two or more refractory components are named as "aged mixture". It is worth noting that "refractory" refers to the refractory particles without S-rich and OM.". Please refer to lines 188-190.

4. Lines 167-168: I recommend bringing Figure S1 into the main paper.

Thanks for your suggestion. Figure S1 has been moved to the main text, and is numbered as Figure 3.

5. Lines 168-169: Not sure what is meant by "influenced by air masses". More description of the different conditions and air mass conditions encountered for each cloud event will help the authors interpret their single particle findings.

To make it clear, "influenced by air masses" has been removed, and we moved the content about the influence of air masses on the distribution of particle types in the RES in the SI to the main text. Please refer to Lines 200-212:

   "The different air masses are expected to affect the distribution of particle types. The distribution of several types of particles in the RES were observed to be divergent in different cloud events, corresponding to different air masses, as shown in Figure 3 and Figure 4. The number fraction of OM-containing particles was the highest (81%) in cloud event #2, which might be partly attributed to the higher concentration of O3 during cloud event #2 (Table S1). And the samples of cloud event #2 sampled at noon. Higher solar radiation at the sampling time might also promote heterogeneous photochemical oxidation reactions during the cloud process and increased the generation of OM within cloud droplets (Xu et al., 2017). Aged metal particles accounted a similar percentage (7-12%) for three cloud events. The proportion of aged mineral during cloud event #1 (14%) was nearly four times those in the other two cloud events. Aged fly ash particles had the highest proportion (10%) in cloud event #3 compared with the other two cloud events, which is most probably influenced by the different air masses (Figure 4). Aged mineral particles of cloud event #1 may be influenced by the long-distance transportation of dust from Southeast Asia (Salam et al., 2003). Clearly, aged fly ash particles of cloud event #3 are associated with the air

masses from the PRD region with a dense distribution of industrial facilities there (Cao et al., 2006)."

6. Lines 171-172: What is meant by "as confirmed by SPAMS data"?

That sentence has been removed in the revised manuscript.

7. Line 176: what is meant by "part of"? Can this be made more quantitative?

Since aged refractory and aged mixture particles include S/S-OM/OM-refractory and S/S-OM/OM-soot/mineral/metal/fly ash. OM-containing particles refer to S-OM/OM-refractory and S-OM/OM-soot/mineral/metal/fly ash, which is part of aged refractory and aged mixture particles. In the RES and INT during cloud event #2 and #3, OM-containing particles account for 63% and 32% of the aged refractory particles and 51% and 43% of the aged mixture particles.

8. Figure 3, should "coating" be "thin coating" instead to better distinguish the morphology?

Thanks for your suggestion. We have changed the mixing structure "coating" to "thinly coated" in the full text and SI.

9. I found the coating thickness definitions to be confusing especially because they overlap. I'm not quite sure how the coating thickness was used to robustly distinguish particles classified as "coating" vs "core-shell".

The electron beam of TEM penetrates the particle, and the internal structure of the particle can be observed (Li et al., 2016). Thus, although the organic matter wraps the internal material, the organic coating and shell can still be easily identified. The major difference between "coating (that is thinly coated now)" and "core-shell" is the relative

thickness of organic coating and shell in the particle is. Core-shell structure possessed thicker organics than thinly coated structure, and the thickness of OM-coating and OM-shell is 12-150 nm and 86-2110 nm in this study, respectively. Please refer to Lines 218-224.

Reference:

Li, W., Sun, J., Xu, L., Shi, Z., Riemer, N., Sun, Y., Fu, P., Zhang, J., Lin, Y., Wang, X., Shao, L., Chen, J., Zhang, X., Wang, Z., and Wang, W.: A conceptual framework for mixing structures in individual aerosol particles, Journal of Geophysical Research-Atmospheres, 121, 13784-13798, 10.1002/2016jd025252, 2016.

10. Lines 219-222 imply that the site is polluted, but the site was presented as a background site.

We are sorry for the misunderstanding. As we described, the results of this study are similar to those of unpolluted remote areas, but different from those in polluted areas. The original sentence has been changed from "Such a mixing structure is similar to those observed in the Arctic, background, or rural atmosphere (Hiranuma et al., 2013; Li et al., 2016; Yu et al., 2019), but is different from previous findings in polluted air where OM is typically mixed with sulfate (Li et al., 2016)." to "Such a mixing structure is similar to those observed in the Arctic, background, or rural atmosphere (Hiranuma et al., 2013; Li et al., 2016; Yu et al., 2019), but is different from other findings in polluted areas where OM is typically mixed with sulfate (Li et al., 2016)."

11. Line 223: reword "follow up strong interactions" to "heterogeneous and multiphase reactions"

It has been changed accordingly.

12. Lines 225-227 seem to imply that there is more data that was not presented. Please

rephrase.

Thanks for pointing out this. The sentence has been changed to "Recently, Gorkowski et al. (2020) came up with a particle morphology prediction framework developed for mixtures of organic aerosol based on the measurements from aerosol optical tweezers experiments and literature data, and they hypothesized the core-shell morphology dominated by secondary organic aerosols (SOA) in the shell phase.". Please refer to lines 262-265.

13. I'm very confused as to how the O/C ratios were determined. Perhaps I missed something, but I thought that the detector used only detected elements heavier than C and it is not clear how the background from the carbon film is accounted for.

The O/C value is measured by EDS (energy-dispersive X-ray spectrometry), which can obtain the weight and atomic number proportion of elements heavier than carbon ($Z \geqslant$ 6), and some limitations of O/C have also been expressed in the main text. Please refer to lines 266-271:
"It should be noted that the O/C ratio of organic coating and shell is underestimated herein due to the copper grid evenly covered by carbon film. And, while some loss of volatile organic compounds during the TEM/EDS analysis may affect the O/C of particles, the relatively higher O/C ratio for the RES is still affirmative. Droplets are expected to dissolve more abundance of volatile organic compounds (Chakraborty et al., 2016), evaporation of which would result in an underestimate of O/C to a higher degree rather than the INT."

14. One of the main conclusions of this paper is regarding oxidized coatings formed via aqueous chemistry, yet the main table showing this is in the SI. I suggest bringing Table S2 into the main paper.

Thanks for your suggestion. Table S2 has been moved to the main text, and numbered as Table 2.

15. The O/C values should be stated in the main paper.

The O/C value of organic shell and coating has been in the main text. Please refer to lines 271-274:

"We found that the average value of the O/C ratio of RES is higher than INT, and the average value of the O/C ratio of RES with core-shell structure is 0.23, which is two times that with thinly coated structure (0.11) (Table 2), indicating that these RES with core-shell particles are more oxidized."

16. Lines 242-245: If ion peak ratios from SPAMS are discussed, then SPAMS must be included in the methods section and the interpretation of the ion peak ratios needs much more interpretation to connect to the data presented in this paper.

We agree with your comment. The operating principle of the SPAMS has been added in the method section (section 2.4), and the introduction of the relative peak area is also described, that is "The relative peak area of characteristic peaks of specific material in the mass spectra is generally applied to indicate its relative abundance in the particle.".

17. Line 251: also site [Moffet and Prather, 2009]

It has been added in the text. Please refer to line 289.
Lines 288-290: While some previous studies demonstrated that soot aggregates tend to be more compact (with larger D_f) after aging or cloud processing (Adachi and Buseck, 2013; Wu et al., 2018; Moffet and Prather, 2009), our results suggest that in-cloud processes may result in more branched soot, as shown in Figure 6.

Reference:

Moffet, R. C., and Prather, K. A.: In-situ measurements of the mixing state and optical properties of soot with implications for radiative forcing estimates, Proceedings of the National Academy of Sciences of the United States of America, 106, 11872-11877, 10.1073/pnas.0900040106, 2009.

18. Lines 254-256: I don't follow the logic regarding non-volatile material and branching. I suggest that the authors more clearly present this argument.

Thank you for pointing out this. We have described that in detail. The sentences have been changed to "The first and the most likely reason is that some of the soot aggregates are immediately encapsulated by non-volatile materials (such as organic matter) after emission by combustion sources. These coatings fill the spaces between the branches of soot aggregates, which inhibits the relatively large deformation and reconfiguration of the soot aggregates during transport and activation into cloud droplets (Zhang et al., 2018). Differently, soot aggregates may shrink easily and become more compact during long-distance transport, if the soot aggregates are emitted without non-volatile coatings (Adachi and Buseck, 2013)." Please refer to lines 292-298.

19. Lines 258-260: could this just be showing the role of particle size where unaged soot is larger and more CCN active than smaller, aged particles?

We are sorry for the misunderstanding. We described the D_f (fractal dimension) of soot particles in the RES and INT in the section 3.2, which is 1.82 ± 0.05 and 2.16 ± 0.05, respectively. And here, we described the ECD (equivalent circle diameter) of soot particles in the RES and INT, which is 266 nm and 247 nm. So, compared with soot in the RES, soot in the INT particles have larger D_f and smaller ECD. To be more clear, the sentence has been changed to "We show that soot aggregates have higher D_f and lower average ECD in the INT (247 nm) than in the RES (266 nm), which means that larger, less dense soot particles are easier to act as CCN.". Please refer to lines 298-300.

20. Lines 268-270: is there a figure showing the off-center positions of the soot?

Yes. The Figure S4 (a, b, c, g) show the off-center positions of the soot. "Figure S4" is added in the sentence. Please refer to lines 307-309:

"Our observations at the background site show that the majority of soot aggregates in both RES and INT (~80%) are located in off-center positions (Figure S4), having less compact shapes even after being coated."

References:

Moffet, R. C., and K. A. Prather (2009), In-situ measurements of the mixing state and optical properties of soot with implications for radiative forcing estimates, Proceedings of the National Academy of Sciences of the United States of America, 106(29), 11872-11877.

Spencer, M. T., and K. A. Prather (2006), Using ATOFMS to determine OC/EC mass fractions in particles, Aerosol Science and Technology, 40(8), 585-594.

Impact of in-cloud aqueous processes on the chemical compositions and morphology of individual atmospheric aerosols

Yuzhen Fu[1, 2], Qinhao Lin[1, #], Guohua Zhang[1, 3, *], Yuxiang Yang[1, 2], Yiping Yang[2, 4], Xiufeng Lian[1, 2], Long Peng[1, 2], Feng Jiang[1, 2, ##], Xinhui Bi[1, 3, *], Lei Li[5], Yuanyuan Wang[6], Duohong Chen[7], Jie Ou[8], Xinming Wang[1, 3], Ping'an Peng[1, 3], Jianxi Zhu[4], Guoying Sheng[1]

[1] State Key Laboratory of Organic Geochemistry and Guangdong Key Laboratory of Environmental Protection and Resources Utilization, Guangzhou Institute of Geochemistry, Chinese Academy of Sciences, Guangzhou 510640, PR China

[2] University of Chinese Academy of Sciences, Beijing 100049, PR China

[3] Guangdong-Hong Kong-Macao Joint Laboratory for Environmental Pollution and Control, Guangzhou 510640, PR China

[4] CAS Key Laboratory of Mineralogy and Metallogeny & Guangdong Provincial Key Laboratory of Mineral Physics and Materials, Guangzhou Institute of Geochemistry, CAS, Guangzhou 510640, PR China

[5] Institute of Mass Spectrometer and Atmosphere Environment, Jinan University, Guangzhou 510632, PR China

[6] Department of Atmospheric Science, School of Earth Science, Zhejiang University, Hangzhou 310027, PR China

[7] State Environmental Protection Key Laboratory of Regional Air Quality Monitoring, Guangdong Environmental Monitoring Center, Guangzhou 510308, PR China

[8] Shaoguan Environmental Monitoring Center, Shaoguan 512026, PR China

[#] now at: Guangdong Key Laboratory of Environmental Catalysis and Health Risk Control, Guangzhou Key Laboratory Environmental Catalysis and Pollution Control, School of Environmental Science and Engineering, Institute of Environmental Health and Pollution Control, Guangdong University of Technology, Guangzhou 510006, PR China.

[##] now at: Institute of Meteorology and Climate Research, Karlsruhe Institute of Technology, Eggenstein-Leopoldshafen 76344, Germany.

Correspondence to: Guohua Zhang (zhanggh@gig.ac.cn) and Xinhui Bi (bixh@gig.ac.cn)

Abstract. The composition, morphology, and mixing structure of individual cloud residues (RES) and interstitial particles (INT) at a mountain-top site were investigated. Eight types of particles were identified, including sulfate-rich (S-rich), S-organic matter (OM), aged soot, aged mineral, aged fly ash, aged metal, refractory, and aged mixture. A shift of dominant particle types from S-rich (29%) and aged soot (27%) in the INT to S-OM (24%) and aged mixture (22%) in the RES is observed. In particular, particles with organic shells are enriched in the RES (30%) relative to the INT (12%). Our results highlight that the formation of more oxidized organic matter in the cloud contributes to the existence of organic shells after cloud processing. We also show that in-cloud processes may result in less compact soot, with the fractal dimensions (D_f) of soot in the RES (1.82 ± 0.12) lower than those in the INT (2.11 ± 0.09). This research emphasizes the role of in-cloud processes on the chemistry and microphysical properties of individual particles. Given that organic coatings may determine the particle hygroscopicity, activation ability, and heterogeneous chemical reactivity, the increase of OM-shelled particles upon in-cloud processes should have considerable implications.

1 Introduction

Aerosol-cloud interaction is regarded as one of the most significant sources of uncertainty in assessing the radiative forcing of aerosols so far (IPCC, 2013). On the one hand, aerosols can participate in the formation of cloud droplets, which is primarily influenced by their chemical composition and size at a certain supersaturation (Fan et al., 2016; Maskey et al., 2017; Ogawa et al., 2016; Raymond and Pandis, 2002; Zelenyuk et al., 2010). On the other hand, in-cloud processes, including the formation of sulfate, nitrate, and water-soluble organics, and the physical processes such as collision and coagulation, would substantially change the physical and chemical properties of the activated particles (Kim et al., 2019; Ma et al., 2013; Roth et al., 2016; Wu et al., 2013). Given that the morphology and mixing state are vital in determining the optical properties of particles (Adachi et al., 2010; Wu et al., 2018), changes of these properties upon in-cloud processes would further affect the subsequent atmospheric processes (e.g., cloud activation, heterogeneous reactions) and radiative forcing of particles after droplet evaporation.

Understanding the morphology and mixing state of particles upon in-cloud processes is of considerable significance to improve the knowledge of aerosol-cloud interactions. For instance, Zelenyuk et al. (2010) found that both cloud droplet residues (RES) and interstitial particles (INT, or unactivated particles in the cloud) are mainly composed of organics, sulfate, biomass burning particles, and processed sea salt at the North Slope of Alaska. Kamphus et al. (2010) observed that 92% of RES are particles containing sulfates, organics, and nitrate at the Jungfraujoch (Swiss Alps). At Mt. Tai, Liu et al. (2018b) observed that main particle types are S (sulfate)-soot (36%), S-fly ash/metal-soot (26%) and S-rich (24%) for RES and S-rich (61%), S-soot (15%) and soot (15%) for INT. These results indicate that both RES and INT present complex mixtures, and carbonaceous matter (i.e., organic materials (OM) and soot) is important material in the cloud mass.

While there are extensive studies reporting the extent of aqueous phase processing on the modification of aerosol bulk (e.g., mass) and/or chemical (e.g., mixing state, hygroscopicity) properties (Chakraborty et al., 2016; Ervens et al., 2011), the influence of in-cloud processes on the physical properties (e.g., shape, mixing structure) of individual particles is still ambiguous. In particular, physical properties can become dominant in the role of cloud activation for particles with inorganic/organic mixed (Topping et al., 2007). A hydrophobic organic-rich coating will form on a hygroscopic particle core if liquid-liquid phase separation occurs (Song et al., 2013). Besides, the distribution of organics and its association with other aerosol types is also crucial for the correct calculation of its radiative effects (Zhu et al., 2017). However, to what extent in-cloud processes play a role in reshaping the distribution of organic and inorganic compositions remains unknown, although such coating structures have been identified in ambient aerosols (Adachi and Buseck, 2008; Li and Shao, 2010; Yu et al., 2019). Considering that in-cloud processes contribute to a substantial fraction (up to 60%) of organic aerosols (Ervens et al., 2011; Liu et al., 2012; Myriokefalitakis et al., 2011; Spracklen et al., 2011), the influence of this process in atmospheric chemistry cannot be neglected.

For another type of carbonaceous material, soot, there is extensive evidence that the absorption and cloud activation of soot-containing particles can be significantly affected by coatings (Adachi et al., 2010; Wu et al.,

79　2018; Moffet and Prather, 2009). The critical factors to accurate predicting of such impact include the amount and

80　nature of the coating material, the exact particle morphology, and the size distribution (Qiu et al., 2012; Radney

81　et al., 2014). Fractal dimension (D_f) is widely used to indicate the extent of branching of soot (Brasil et al., 1999),

82　with densely packed or compacted soot particles having higher D_f than chain-like branched clusters or open

83　structures. While some studies have found that soot restructuring occurs after water processing (Bhandari et al.,

84　2019; Ma et al., 2013; Mikhailov et al., 2006), or being coated by OM (Spencer and Prather, 2006) and sulfate

85　(Zhang et al., 2008), Khalizov et al. (2013) suggested that soot with thin organic coating did not become more

86　compact under high humidity. However, the morphology and mixing structure of soot involving the formation of

87　organics upon cloud processing is also poorly constrained because of the limited field observation.

88　　To further improve our understanding of the morphology and mixing structures between the various

89　components within individual RES and INT, we conducted a 25-day field observation of cloud events at a

90　background site in southern China. A transmission electron microscope (TEM) combined with energy-dispersive

91　X-ray spectrometry (EDS) was used to analyze the chemical composition, size, morphology, and mixing structure

92　of individual RES and INT. Previously, the chemical composition and mixing state of RES at the same site have

93　been investigated with a single particle aerosol mass spectrometer (SPAMS) (Lin et al., 2017; Zhang et al., 2017a).

94　Herein, we focus on the mixing structure (e.g., chemical compositions and morphology) of individual particles,

95　in particular, OM-containing particles. Meanwhile, particle types and mixing state of RES and INT are also

96　discussed. The difference between the mixing structure of RES and INT may indicate the impact of in-cloud

97　aqueous processes.

2 Materials and Methods

2.1 Sampling site

100　　Sampling was conducted at the top of Mt. Tianjing (112°53′56″ E, 24°41′56″ N; 1690 m above sea level) in

101　southern China from 18 May to 11 June 2017. The sampling site is located in a natural preserve, and it is almost

102　unaffected by local anthropogenic sources. It is about 50 km and 350 km away from the north of the Pearl River

103　Delta (PRD) region and the South China Sea, respectively.

2.2 Collection of RES and INT

105　　A cloud event was identified with visibility below a threshold of 3 km and relative humidity (RH) above a

106　threshold of 95%, using a ground-based counterflow virtual impactor (GCVI, model 1205, Brechtel Mfg. Inc.,

107　USA). The GCVI was automatically triggered when there was a cloud event, whereas it was not allowed to sample

108　when a precipitation sensor detected rain or snow. Then cloud droplets were introduced into the GCVI, followed

109　by removing water in an evaporation chamber (40 ℃) to obtain RES. The sampling process might experience

110　some particle loss due to the evaporation of highly volatile substances. The droplet cut size, at which the

111　transmission efficiency of CVI was 50%, was set at a size larger than 7.5 μm (Shingler et al., 2012). INT was

112　sampled using another inlet (PM$_{2.5}$ cyclone inlet, 5 lpm), followed by passing through a silica gel diffusion dryer.

A DKL-2 sampler (Genstar Electronic Technology Co., Ltd., China) was used to collect RES and INT on copper grids coated with carbon film with an airflow of 1 L min^{-1}. The collection efficiency of the sampler is 50% at 80 nm, assuming the particle density is 2 g cm^{-3}. To avoid particle overlapping, the sampling duration was set within 10 minutes. All samples were placed in a sealed plastic sample box and stored in a desiccator at room temperature for subsequent analysis.

The information about cloud events and samples are summarized in Table 1. We focused on three cloud events (#1, #2, and #3), with a duration of 14, 34, and 47 hours, respectively. RES and INT samples from these cloud events were analyzed, with INT not available for the cloud event #1. To minimize the influence of rapid change of cloud condition, all the samples were collected during the stable and mature periods (Visibility < 100 m).

2.3 TEM analysis of RES and INT

Chemical composition, size, and morphology of individual RES and INT were characterized by a TEM (FEI Talos F200S) operated at 200 kV. TEM/EDS is a very effective tool to analyze the microscopic characteristics of individual particles. The resolution of images between 1 μm and 100 nm can be magnified from 7,000 to 36,000 fold, which depended on the size of particles. The EDS is coupled with TEM to detect the intensity of elements heavier than carbon ($Z \geq 6$). The produced X-rays signal in the EDS system is detected by a silicon (Si) drift detector (SSD), and thus Si is not considered in the discussion. Cu is also not considered due to the interference from the copper grids. In the TEM vacuum chamber, some volatile substances (e.g., ammonium nitrate (NH_4NO_3) and volatile organic matter) would be lost. Moreover, volatile materials are often sensitive to strong electron beams. Due to the analysis error of volatile materials, TEM/EDS studies typically focus on refractory compositions. Using an image analysis software (ImageJ), the equivalent circle diameters (ECD) of all particles can be obtained from the scanned images from the TEM. For particles with rim, only the nucleus is counted, because the rims contain only a small amount of OM. Overall, 780 particles, including RES and INT, were analyzed.

Base on various element spectra, RES and INT were mainly classified as sulfate-rich (S-rich), carbonaceous material, mineral, metal, and fly ash (Twohy and Anderson, 2008; Li et al., 2016). Elemental compositions of S-rich were dominated by S and O, and some of them were associated with minor N, K and Na. Low intensity of N could be due to the evaporation of ammonia nitrate under the high energy electron beam (Smith et al., 2012). This led to the bubbly appearance of S-rich. In this case, S-rich represented secondary inorganic particles. The elemental compositions of carbonaceous materials were characteristics of abundant C and minor O. Carbonaceous materials were divided into soot and OM according to different morphology. Soot were composed of tens to hundreds of carbon spheres ranging from 21 to 108 nm in diameter (average diameter was 47.7 nm), which often displayed botryoidal aggregates. OM did not have chain-like structure, which generally exhibited amorphous state and spherical or irregular shapes. Mineral particles were consisted of Si, Al, Ca, O and minor Fe. Mineral were mainly clay, feldspar, calcite and gypsum, usually showing irregular shapes. Metal particles were represented as Fe, Zn, Ti, Mn, or Ni. Metal particles were characteristic of spherical, rectangular or irregular morphologies. They were largely from natural dust and industrial combustion (Silva et al., 2000; Ye et al., 2018). The presence of spherical metal particles indicated that they experienced melting at high temperature (Giere et al., 2003; Giere et

150 al., 2006). Fly ash particles mainly contained Si, Al and O. Fly ash particles tended to be spherical in morphology
151 and they were generally produced from the process of coal combustion (Chen et al., 2012; Henry and Knapp,
152 1980).

153 **2.4 SPAMS analysis of RES and INT**

154 A SPAMS (Hexin Analytical Instrument Co., Ltd., Guangzhou, China) was used to analyze chemical
155 composition and size distribution of individual particles in real-time. Particles entering SPAMS were first focused
156 into a beam of particles, and then their vacuum dynamic size (D_{va}) were measured by two continuous diode
157 Nd:YAG laser beams (532 nm). Next, the pulsed laser (266 nm) was precisely triggered to ionize target particle
158 according to the intrinsic velocity of each particle. Finally, we obtained the information of individual particles
159 including vacuum dynamic particle size and the positive and negative ion mass spectrometry. The relative peak
160 area of characteristic peaks of specific material in the mass spectra is generally applied to indicate its relative
161 abundance in the particle.

162 **2.5 Calculating morphology parameters of soot**

163 The fractal dimension of soot is characterized in the following statistical scaling law (Brasil et al., 1999; Köylü
164 et al., 1995):

165
$$N = k_g \left(\frac{2R_g}{d_p}\right)^{D_f}$$

166 where N is the number of monomers within a certain soot aggregate, k_g is the fractal pre-factor, R_g is the radius of
167 gyration, d_p is the diameter of the monomer, and D_f is the mass fractal dimension. R_g can be obtained by using a
168 simple relationship between R_g and L_{max}, the maximum length of the soot aggregate (Brasil et al., 1999):

169
$$L_{max}/2R_g = 1.50 \pm 0.05$$

170 And, the number of monomers, N, can be calculated by a power-law correlation of projected area of monomer
171 and aggregate:

172
$$N = k_a \left(\frac{A_a}{A_p}\right)^{\alpha}$$

173 where k_a is a constant, A_a and A_p are the projected area of aggregate and monomer, respectively, and α is an
174 empirical projected area exponent. The value of k_a and α depends on the degree of monomer overlap (δ) in the
175 aggregate (Oh and Sorensen, 1997), and δ can be determined by:

176
$$\delta = \frac{2a}{l}$$

177 where *a* is monomer radius, and *l* is the center distance of adjacent monomers. The value of parameters including

178 *a*, *l*, A_a, A_p, L_{max}, and d_p can be obtained by analyzing TEM images. Then D_f can be calculated by the above four

179 formulas.

180 **3 Results and Discussion**

181 **3.1 Particle type and mixing state of RES and INT**

182 According to mixing state, RES and INT were divided into following eight types (Figure 1): S-rich, S-OM,

183 refractory (soot/mineral/metal/fly ash), aged soot (S/OM-soot), aged mineral (S/OM-mineral), aged metal (S/OM-

184 metal), aged fly ash (S/OM-fly ash), and aged mixture (S/OM-soot/mineral/metal/fly ash). S-rich or OM, generally

185 considered to be aged since they are mainly secondarily produced in the atmosphere, are internally mixed with

186 refractory materials (soot/mineral/metal/fly ash) (Canagaratna et al., 2007; Huang et al., 2012; Jiang et al., 2019).

187 Such internally mixed S/OM-refractory particles are named as aged refractory particles herein. Aged particle types

188 containing two or more refractory components are named as "aged mixture". It is worth noting that refractory are

189 refractory particles without S-rich and OM.

190 Figure 2 shows the number fraction of different particle types in the RES and INT during cloud events #2 and

191 #3. S-rich, S-OM, aged soot, and aged mixture particles are dominant particle types. The most abundant particles

192 in the RES are aged mixture (23%), followed by S-OM (22%), aged soot (20%), S-rich (16%), aged metal (9%),

193 aged fly ash (5%), aged mineral (4%), and refractory (1%). Differently, INT is predominated by S-rich (29%),

194 aged soot (27%), S-OM (15%), aged mixture (10%), and the lesser percentage of aged fly ash (8%), refractory

195 (5%), aged mineral (4%), and aged metal (2%) were also observed. Among three cloud events, the RES are

196 dominated by S-OM in cloud event #1 and #2 and aged mixture particles in cloud event #3 (Figure 3). It is also

197 shown that the RES and INT analyzed by TEM/EDS can represent their compositions throughout cloud events #2

198 and #3, since such compositions were relatively stable throughout these periods (Figure S3).

199 The different air masses are expected to affect the distribution of particle types. The distribution of several types

200 of particles in the RES were observed to be divergent in different cloud events, corresponding to different air

201 masses, as shown in Figure 3 and Figure 4. The number fraction of OM-containing particles was the highest (81%)

202 in cloud event #2, which might be partly attributed to the higher concentration of O_3 during cloud event #2 (Table

203 S1). And the samples of cloud event #2 sampled at noon. Higher solar radiation at the sampling time might also

204 promote heterogeneous photochemical oxidation reactions during the cloud process and increased the generation

205 of OM within cloud droplets (Xu et al., 2017). Aged metal particles accounted a similar percentage (7-12%) for

206 three cloud events. The proportion of aged mineral during cloud event #1 (14%) was nearly four times those in

207 the other two cloud events. Aged fly ash particles had the highest proportion (10%) in cloud event #3 compared

208 with the other two cloud events, which is most probably influenced by the different air masses (Figure 4). Aged

209 mineral particles of cloud event #1 may be influenced by the long-distance transportation of dust from Southeast

210 Asia (Salam et al., 2003). Clearly, aged fly ash particles of cloud event #3 are associated with the air masses from

211 the PRD region with a dense distribution of industrial facilities there (Cao et al., 2006).

3.2 The morphology and mixing structure of carbonaceous particles

OM-containing particles, including all of S-OM particles, part of aged refractory (S-OM/OM-refractory) and aged mixture (S-OM/OM-soot/mineral/metal/fly ash) particles, accounted for 60% of RES and 33% of INT during cloud events #2 and #3. According to the mixing structures between OM and other materials (Figure 5), OM-containing particles are classified into the following five categories: thinly coated (Figure 5b), core-shell (Figure 5c), embedded (Figure 5d), attached (Figure 5e) and homogenous-like (Figure 5f) structures (Li et al., 2016). A particle is classified as thinly coated structure when wrapped with a thin layer of OM. The thickness of the OM layer of thinly coated particles ranges from 12 to 150 nm. Generally, the shapes of OM-containing particles with thinly coated structure are elliptical or irregular. The difference between the core-shell structure and thinly coated structure is the relative thickness of OM: Core-shell structure possessed thicker organics than thinly coated structure. The thickness of the shell varies from 86 to 2110 nm, and the ratio of the projected area of the shell to particle ranges from 0.20 to 0.97. Moreover, OM-containing particles with core-shell structure are round. Embedded structure refers to the particle with OM embedded in other materials (e.g., sulfate). The attached structure refers to the particle of OM attached to other materials. The homogenous-like structure represents particles with evenly mixed and no identifiable boundary between organic and non-organic matter.

The first most abundant particles are thinly coated geometry, comprising 53% of RES and 59% of INT during cloud event #2 and #3, respectively. The second are core-shell particles for RES and attached particles for INT. The percentage of core-shell particles in the RES is almost 2.5 times that in the INT (27% vs. 12%). Embedded and homogenous-like particles account for minor proportions (< 4%) for both RES and INT.

Soot-containing particles, including all of aged soot particles (S/OM-soot) and part of refractory (soot/mineral/metal/fly ash) and aged mixture particles (S/OM-soot/mineral/metal/fly ash), account for 36% of RES and 39% of INT during cloud event #2 and #3, respectively. The fraction is consistent with the range of those (< 30% – ~60%) observed at the same site by SPAMS (Zhang et al., 2017a). Most of the soot are distributed around the periphery of particles (Figure S4). Figure 6 shows the D_f of soot within RES and INT of cloud event #2 and #3. The result shows that the D_f of soot is smaller in the RES (1.82 ± 0.12) than in the INT (2.11 ± 0.09), which means that soot is more branched in the RES. It is noted that 62.5% of all soot-containing particles with clear boundaries are included in the D_f calculation since thick coating around soot might make the boundary of monomers not clear enough (Bhandari et al., 2019). The obtained D_f are close to those ($1.83 – 2.16$) reported at a background site (Wang et al., 2017). The D_f of soot in the RES and INT likely represents partly coated soot (1.82 ± 0.05) (Yuan et al., 2019) and embedded soot (2.16 ± 0.05) (Wang et al., 2017), respectively. In addition to emission sources and coating processes, high relative humidity (RH) during nighttime is a critical factor to increase the compactness of soot (Yuan et al., 2019).

3.3 In-cloud formation of OM

It can be seen from Figure 2 that a shift of dominant particle types from S-rich (29%) and aged soot (27%) in the INT to the aged mixture (23%) and S-OM (22%) in the RES. In particular, the fraction of OM-containing particles increases from 33% in the INT to 60% in the RES. It is unlikely due to the favorable activation of S-OM or aged mixture, since mixing with OM generally lower the hygroscopicity of inorganic-dominant particles (e.g.,

249   S-rich) (Brooks et al., 2004; Pierce et al., 2012). OM coating at the same site has been shown to inhibit the CCN

250   activation of soot-containing particles (Zhang et al., 2017a). Instead, it is most probably attributed to the in-cloud

251   formation of OM on the surface of some S-rich particles, shifting the dominant particle type from S-rich to S-OM

252   particles. It can be supported by the relatively larger median size of S-OM particles (0.76 μm) than S-rich particles

253   (0.56 μm) (Figure S5), since in-cloud formation of OM is expected to enlarge the original S-rich particles (Pierce

254   et al., 2012).

255   In addition, the fraction of OM-containing particles with core-shell mixing structure in the RES is almost 2.5

256   times that in the INT (Figure 5a). Such a mixing structure is similar to those observed in the Arctic, background,

257   or rural atmosphere (Hiranuma et al., 2013; Li et al., 2016; Yu et al., 2019), but is different from other findings in

258   polluted areas where OM is typically mixed with sulfate (Li et al., 2016). It is also consistent with several

259   laboratory simulations demonstrating that reactive uptake of volatile organic compounds (VOCs) on inorganic

260   sulfate and heterogeneous and multiphase reactions between there species would lead to a core-shell morphology

261   (e.g., Zhang et al., 2018; Riva et al., 2019; Zhang et al., 2019). Recently, Gorkowski et al. (2020) came up with a

262   particle morphology prediction framework developed for mixtures of organic aerosol based on the measurements

263   from aerosol optical tweezers experiments and literature data, and they hypothesized the core-shell morphology

264   dominated by secondary organic aerosols (SOA) in the shell phase.

265   Moreover, we estimated the O/C ratio of coating and shell within OM-containing particles. It should be noted

266   that the O/C ratio of organic coating and shell is underestimated herein due to the copper grid evenly covered by

267   carbon film. And, while some loss of volatile organic compounds during the TEM/EDS analysis may affect the

268   O/C of particles, the relatively higher O/C ratio for the RES is still affirmative. Droplets are expected to dissolve

269   more abundance of volatile organic compounds (Chakraborty et al., 2016), evaporation of which would result in

270   an underestimate of O/C to a higher degree rather than the INT. We found that the average value of the O/C ratio

271   of RES is higher than INT, and the average value of the O/C ratio of RES with core-shell structure is 0.23, which

272   is two times that with thinly coated structure (0.11) (Table 2), indicating that these RES with core-shell particles

273   are more oxidized. At the same site, we have previously observed enhanced aqueous SOA, such as oxalate in the

274   cloud (Zhang et al., 2017b). Higher O/C ratio of core-shell particles is also consistent with current studies reporting

275   more oxidized organic species in cloud/fog residues (Brege et al., 2018; Chakraborty et al., 2016; Zhang et al.,

276   2017b). With high levels of VOCs at the sampling site (Lv et al., 2019), prevalent formation of aqueous SOA

277   through the uptake of VOCs in cloud droplets would be expected (Kim et al., 2019; Liu et al., 2018a). The

278   contribution from photochemical processes may also be reflected by the association of the highest fraction (81%)

279   of OM-containing particles with a higher concentration of O_3 during cloud event #2 (Table S1).

280   However, one may expect that such core-shell mixing structure in the RES can also be explained by the primary

281   activation of S-OM particles with larger sizes. Unfortunately, no sample is available before cloud events. However,

282   with evidence from the collocated SPAMS, we show that this is not convincing. As shown in Table S2, the ratios

283   of relative peak area between organics and sulfate are similar between the INT and particles before cloud event,

284   whereas they are higher in the RES. This is corresponding to the production of oxidized organics during in-cloud

285   processes (Zhang et al., 2017b).

286   **3.4 The D_f of soot in the RES and INT**

287   While some previous studies demonstrated that soot aggregates tend to be more compact (with larger D_f) after
288   aging or cloud processing (Adachi and Buseck, 2013; Wu et al., 2018; Moffet and Prather, 2009), our results
289   suggest that in-cloud processes may result in more branched soot, as shown in Figure 6. Considering that D_f is
290   controlled mainly by emission sources, combustion conditions, and aging processes (Adachi et al., 2007), we
291   propose three possible explanations for the lower D_f of soot in the RES than that in the INT. The first and the most
292   likely reason is that some of the soot aggregates are immediately encapsulated by non-volatile materials (such as
293   organic matter) after emission by combustion sources. These coatings fill the spaces between the branches of soot
294   aggregates, which inhibits the relatively large deformation and reconfiguration of the soot aggregates during
295   transport and activation into cloud droplets (Zhang et al., 2018). Differently, soot aggregates may shrink easily
296   and become more compact during long-distance transport, if the soot aggregates are emitted without non-volatile
297   coatings (Adachi and Buseck, 2013). We show that soot aggregates have higher D_f and lower average ECD in the
298   INT (247 nm) than in the RES (266 nm), which means that larger, less dense soot particles are easier to act as
299   CCN. This is consistent with a study reporting that small particles are more compact than large particles (Adachi
300   et al., 2014). The second is that water-soluble substances within aerosols will be miscible after activating to cloud
301   droplets (Gorkowski et al., 2020), and the coating materials of soot may be released, which makes soot more
302   branched in the droplets and the following-up droplet evaporation. The third possible explanation is that different
303   combustion materials and combustion conditions produce soot-containing particles with different mixing states
304   and morphology (China et al., 2014; Khalizov et al., 2013; Liu et al., 2017; Zhang et al., 2018).

305   This result is in contrast to the current study reporting that soot sampled after cloud droplet evaporating are
306   more compact than freshly emitted and interstitial soot (Bhandari et al., 2019). Our observations at the background
307   site show that the majority of soot aggregates in both RES and INT (~80%) are located in off-center positions
308   (Figure S4), having less compact shapes even after being coated. This is quite different from the core-shell model
309   currently used in the climate models (Bond and Bergstrom, 2006; Wu et al., 2018). Through theoretical calculation,
310   Adachi et al. (2010) suggested that absorption cross-sections could be reduced by 20-30% with off-center
311   positions of soot relative to center positions. This means that the models based on core-shell assumption may
312   overestimate the absorption of soot-containing particles after cloud processing.

313   **4 Conclusion and atmospheric implications**

314   The result highlights the different morphology and mixing structures of activated and interstitial particles,
315   which may imply the substantial role of in-cloud aqueous processes in reshaping the activated particles. While Yu
316   et al. (2019) considered organic coatings on sulfate in the Arctic as a result of the increase of SOA following
317   particle aging and growth during transport, our data further imply a specific role of in-cloud processes in the
318   coating on sulfate. The prevalence of OM shelled particles after cloud processing also supports a current laboratory
319   observation depicting that rapid film formation and fast heterogeneous oxidation can provide an efficient way of
320   converting water-insoluble organic films into more water-soluble components in aerosols or cloud droplets
321   (Aumann and Tabazadeh, 2008).

322   Gorkowski et al. (2020) suggested that mixing structures of OM-containing particles are related to the oxidation
323   degree of OM. We also show that OM shells formed in-cloud have a higher degree of oxidation. Such a chemical

10

and ==morphological== modification of aerosol particles may influence species diffusivities from the interior to the surface region of the shell and gas-particle partitioning between the shell and gas (Liu et al., 2016; Shiraiwa et al., 2013). Such a reshaping may also have an influence on aerosol hygroscopicity. Extrapolating the linear relationship between the O/C ratio and the hygroscopicity parameter (κ_{org}) indicates that $\kappa_{org-shell}$ is about 1.4 times $\kappa_{org-coating}$ (Jimenez et al., 2009; Lambe et al., 2011). In addition, the formation of the organic film could result in a change of surface tension and thus affect the critical supersaturation required for particle activation (Ovadnevaite et al., 2017). For mineral particles, the heterogeneous ice nucleation potential may be suppressed when coated by OM (Möhler et al., 2008). Given the critical contribution of in-cloud aqueous SOA, several mixing structures of OM-containing aerosols upon in-cloud processes may have substantial implications in modeling the direct and indirect radiative forcing of aerosols (Scott et al., 2014; Zhu et al., 2017).

References

Adachi, K., Chung, S. H., Friedrich, H., and Buseck, P. R.: Fractal parameters of individual soot particles determined using electron tomography: Implications for optical properties, Journal of Geophysical Research-Atmospheres, 112, D14202, 10.1029/2006jd008296, 2007.

Adachi, K., and Buseck, P. R.: Internally mixed soot, sulfates, and organic matter in aerosol particles from Mexico City, Atmospheric Chemistry and Physics, 8, 6469-6481, 10.5194/acp-8-6469-2008, 2008.

Adachi, K., Chung, S. H., and Buseck, P. R.: Shapes of soot aerosol particles and implications for their effects on climate, Journal of Geophysical Research-Atmospheres, 115, D15206, 10.1029/2009jd012868, 2010.

Adachi, K., and Buseck, P. R.: Changes of ns-soot mixing states and shapes in an urban area during CalNex, Journal of Geophysical Research-Atmospheres, 118, 3723-3730, 10.1002/jgrd.50321, 2013.

358   Adachi, K., Zaizen, Y., Kajino, M., and Igarashi, Y.: Mixing state of regionally transported soot particles and the
359   coating effect on their size and shape at a mountain site in Japan, Journal of Geophysical Research-Atmospheres,
360   119, 5386-5396, 10.1002/2013jd020880, 2014.

361   Aumann, E., and Tabazadeh, A.: Rate of organic film formation and oxidation on aqueous drops, Journal of
362   Geophysical Research-Atmospheres, 113, D23205, 10.1029/2007jd009738, 2008.

363   Bhandari, J., China, S., Chandrakar, K. K., Kinney, G., Cantrell, W., Shaw, R. A., Mazzoleni, L. R., Girotto, G.,
364   Sharma, N., Gorkowski, K., Gilardoni, S., Decesari, S., Facchini, M. C., Zanca, N., Pavese, G., Esposito, F.,
365   Dubey, M. K., Aiken, A. C., Chakrabarty, R. K., Moosmüller, H., Onasch, T. B., Zaveri, R. A., Scarnato, B.
366   V., Fialho, P., and Mazzoleni, C.: Extensive Soot Compaction by Cloud Processing from Laboratory and Field
367   Observations, Scientific reports, 9, 11824-11824, 10.1038/s41598-019-48143-y, 2019.

368   Bond, T. C., and Bergstrom, R. W.: Light absorption by carbonaceous particles: An investigative review, Aerosol
369   Science and Technology, 40, 27-67, 10.1080/02786820500421521, 2006.

370   Brasil, A. M., Farias, T. L., and Carvalho, M. G.: A recipe for image characterization of fractal-like aggregates,
371   Journal of Aerosol Science, 30, 1379-1389, 10.1016/s0021-8502(99)00026-9, 1999.

372   Brege, M., Paglione, M., Gilardoni, S., Decesari, S., Facchini, M. C., and Mazzoleni, L. R.: Molecular insights on
373   aging and aqueous-phase processing from ambient biomass burning emissions-influenced Po Valley fog and
374   aerosol, Atmospheric Chemistry and Physics, 18, 13197-13214, 10.5194/acp-18-13197-2018, 2018.

375   Brooks, S. D., DeMott, P. J., and Kreidenweis, S. M.: Water uptake by particles containing humic materials and
376   mixtures of humic materials with ammonium sulfate, Atmospheric Environment, 38, 1859-1868,
377   10.1016/j.atmosenv.2004.01.009, 2004.

378   Canagaratna, M. R., Jayne, J. T., Jimenez, J. L., Allan, J. D., Alfarra, M. R., Zhang, Q., Onasch, T. B., Drewnick,
379   F., Coe, H., Middlebrook, A., Delia, A., Williams, L. R., Trimborn, A. M., Northway, M. J., DeCarlo, P. F.,
380   Kolb, C. E., Davidovits, P., and Worsnop, D. R.: Chemical and microphysical characterization of ambient
381   aerosols with the aerodyne aerosol mass spectrometer, Mass Spectrometry Reviews, 26, 185-222,
382   10.1002/mas.20115, 2007.

383   Cao, G., Zhang, X., and Zheng, F.: Inventory of black carbon and organic carbon emissions from China,
384   Atmospheric Environment, 40, 6516-6527, 10.1016/j.atmosenv.2006.05.070, 2006.

385   Chakraborty, A., Ervens, B., Gupta, T., and Tripathi, S. N.: Characterization of organic residues of size-resolved
386   fog droplets and their atmospheric implications, Journal of Geophysical Research-Atmospheres, 121, 4317-
387   4332, 10.1002/2015jd024508, 2016.

388   Chen, H., Laskin, A., Baltrusaitis, J., Gorski, C. A., Scherer, M. M., and Grassian, V. H.: Coal fly ash as a source
389   of iron in atmospheric dust, Environmental Science & Technology, 46, 2112-2120, 10.1021/es204102f, 2012.

390   China, S., Salvadori, N., and Mazzoleni, C.: Effect of Traffic and Driving Characteristics on Morphology of
391   Atmospheric Soot Particles at Freeway On-Ramps, Environmental Science & Technology, 48, 3128-3135,
392   10.1021/es405178n, 2014.

393   Ervens, B., Turpin, B. J., and Weber, R. J.: Secondary organic aerosol formation in cloud droplets and aqueous
394   particles (aqSOA): a review of laboratory, field and model studies, Atmospheric Chemistry and Physics, 11,
395   11069-11102, 10.5194/acp-11-11069-2011, 2011.

396   Fan, J., Wang, Y., Rosenfeld, D., and Liu, X.: Review of Aerosol-Cloud Interactions: Mechanisms, Significance,
397   and Challenges, Journal of the Atmospheric Sciences, 73, 4221-4252, 10.1175/jas-d-16-0037.1, 2016.

Giere, R., Carleton, L. E., and Lumpkin, G. R.: Micro- and nanochemistry of fly ash from a coal-fired power plant, American Mineralogist, 88, 1853-1865, 10.2138/am-2003-11-1228, 2003.

Giere, R., Blackford, M., and Smith, K.: TEM study of PM2.5 emitted from coal and tire combustion in a thermal power station, Environmental Science & Technology, 40, 6235-6240, 10.1021/es060423m, 2006.

Gorkowski, K., Donahue, N. M., and Sullivan, R. C.: Aerosol Optical Tweezers Constrain the Morphology Evolution of Liquid-Liquid Phase-Separated Atmospheric Particles, Chem, 6, 204-220, 10.1016/j.chempr.2019.10.018, 2020.

Henry, W. M., and Knapp, K. T.: Compound forms of fossil-fuel fly-ash emissions, Environmental Science & Technology, 14, 450-456, 10.1021/es60164a010, 1980.

Hiranuma, N., Brooks, S. D., Moffet, R. C., Glen, A., Laskin, A., Gilles, M. K., Liu, P., Macdonald, A. M., Strapp, J. W., and McFarquhar, G. M.: Chemical characterization of individual particles and residuals of cloud droplets and ice crystals collected on board research aircraft in the ISDAC 2008 study, Journal of Geophysical Research-Atmospheres, 118, 6564-6579, 10.1002/jgrd.50484, 2013.

Huang, H., Ho, K. F., Lee, S. C., Tsang, P. K., Ho, S. S. H., Zou, C. W., Zou, S. C., Cao, J. J., and Xu, H. M.: Characteristics of carbonaceous aerosol in PM2.5: Pearl Delta River Region, China, Atmospheric Research, 104, 227-236, 10.1016/j.atmosres.2011.10.016, 2012.

Intergovernmental Panel on Climate Change (IPCC) (2013), Climate Change 2013: the physical science basis, Cambridge University Press, Cambridge, United Kingdom and New York, NY, USA, 2013

Jiang, F., Liu, F., Lin, Q., Fu, Y., Yang, Y., Peng, L., Lian, X., Zhang, G., Bi, X., Wang, X., and Sheng, G.: Characteristics and Formation Mechanisms of Sulfate and Nitrate in Size-segregated Atmospheric Particles from Urban Guangzhou, China, Aerosol and Air Quality Research, 19, 1284-1293, 10.4209/aaqr.2018.07.0251, 2019.

Jimenez, J. L., Canagaratna, M. R., Donahue, N. M., Prevot, A. S. H., Zhang, Q., Kroll, J. H., DeCarlo, P. F., Allan, J. D., Coe, H., Ng, N. L., Aiken, A. C., Docherty, K. S., Ulbrich, I. M., Grieshop, A. P., Robinson, A. L., Duplissy, J., Smith, J. D., Wilson, K. R., Lanz, V. A., Hueglin, C., Sun, Y. L., Tian, J., Laaksonen, A., Raatikainen, T., Rautiainen, J., Vaattovaara, P., Ehn, M., Kulmala, M., Tomlinson, J. M., Collins, D. R., Cubison, M. J., Dunlea, E. J., Huffman, J. A., Onasch, T. B., Alfarra, M. R., Williams, P. I., Bower, K., Kondo, Y., Schneider, J., Drewnick, F., Borrmann, S., Weimer, S., Demerjian, K., Salcedo, D., Cottrell, L., Griffin, R., Takami, A., Miyoshi, T., Hatakeyama, S., Shimono, A., Sun, J. Y., Zhang, Y. M., Dzepina, K., Kimmel, J. R., Sueper, D., Jayne, J. T., Herndon, S. C., Trimborn, A. M., Williams, L. R., Wood, E. C., Middlebrook, A. M., Kolb, C. E., Baltensperger, U., and Worsnop, D. R.: Evolution of Organic Aerosols in the Atmosphere, Science, 326, 1525-1529, 10.1126/science.1180353, 2009.

Kamphus, M., Ettner-Mahl, M., Klimach, T., Drewnick, F., Keller, L., Cziczo, D. J., Mertes, S., Borrmann, S., and Curtius, J.: Chemical composition of ambient aerosol, ice residues and cloud droplet residues in mixed-phase clouds: single particle analysis during the Cloud and Aerosol Characterization Experiment (CLACE 6), Atmospheric Chemistry and Physics, 10, 8077-8095, 10.5194/acp-10-8077-2010, 2010.

Khalizov, A. F., Lin, Y., Qiu, C., Guo, S., Collins, D., and Zhang, R.: Role of OH-Initiated Oxidation of Isoprene in Aging of Combustion Soot, Environmental Science & Technology, 47, 2254-2263, 10.1021/es3045339, 2013.

437 Kim, H., Collier, S., Ge, X., Xu, J., Sun, Y., Jiang, W., Wang, Y., Herckes, P., and Zhang, Q.: Chemical processing
438   of water-soluble species and formation of secondary organic aerosol in fogs, Atmospheric Environment, 200,
439   158-166, 10.1016/j.atmosenv.2018.11.062, 2019.

440 Köylü, Ü. Ö., Xing, Y. C., and Rosner, D. E.: Fractal morphology analysis of combustion-generated aggregates
441   using angular light scattering and electron microscope images, Langmuir, 11, 4848-4854, 10.1021/la00012a043,
442   1995.

443 Lambe, A. T., Onasch, T. B., Massoli, P., Croasdale, D. R., Wright, J. P., Ahern, A. T., Williams, L. R., Worsnop,
444   D. R., Brune, W. H., and Davidovits, P.: Laboratory studies of the chemical composition and cloud
445   condensation nuclei (CCN) activity of secondary organic aerosol (SOA) and oxidized primary organic aerosol
446   (OPOA), Atmospheric Chemistry and Physics, 11, 8913-8928, 10.5194/acp-11-8913-2011, 2011.

447 Li, W., and Shao, L.: Mixing and water-soluble characteristics of particulate organic compounds in individual
448   urban aerosol particles, Journal of Geophysical Research-Atmospheres, 115, D02301, 10.1029/2009jd012575,
449   2010.

450 Li, W., Sun, J., Xu, L., Shi, Z., Riemer, N., Sun, Y., Fu, P., Zhang, J., Lin, Y., Wang, X., Shao, L., Chen, J., Zhang,
451   X., Wang, Z., and Wang, W.: A conceptual framework for mixing structures in individual aerosol particles,
452   Journal of Geophysical Research-Atmospheres, 121, 13784-13798, 10.1002/2016jd025252, 2016.

453 Lin, Q., Zhang, G., Peng, L., Bi, X., Wang, X., Brechtel, F. J., Li, M., Chen, D., Peng, P. a., Sheng, G., and Zhou,
454   Z.: In situ chemical composition measurement of individual cloud residue particles at a mountain site, southern
455   China, Atmospheric Chemistry and Physics, 17, 8473-8488, 10.5194/acp-17-8473-2017, 2017.

456 Liu, F., Bi, X., Zhang, G., Lian, X., Fu, Y., Yang, Y., Lin, Q., Jiang, F., Wang, X., Peng, P., and Sheng, G.: Gas-
457   to-particle partitioning of atmospheric amines observed at a mountain site in southern China, Atmospheric
458   Environment, 195, 1-11, 10.1016/j.atmosenv.2018.09.038, 2018a.

459 Liu, J., Horowitz, L. W., Fan, S., Carlton, A. G., and Levy, H., II: Global in-cloud production of secondary organic
460   aerosols: Implementation of a detailed chemical mechanism in the GFDL atmospheric model AM3, Journal of
461   Geophysical Research-Atmospheres, 117, D15303, 10.1029/2012jd017838, 2012.

462 Liu, L., Kong, S., Zhang, Y., Wang, Y., Xu, L., Yan, Q., Lingaswamy, A. P., Shi, Z., Lv, S., Niu, H., Shao, L.,
463   Hu, M., Zhang, D., Chen, J., Zhang, X., and Li, W.: Morphology, composition, and mixing state of primary
464   particles from combustion sources - crop residue, wood, and solid waste, Scientific Reports, 7, 5047,
465   10.1038/s41598-017-05357-2, 2017.

466 Liu, L., Zhang, J., Xu, L., Yuan, Q., Huang, D., Chen, J., Shi, Z., Sun, Y., Fu, P., Wang, Z., Zhang, D., and Li,
467   W.: Cloud scavenging of anthropogenic refractory particles at a mountain site in North China, Atmospheric
468   Chemistry and Physics, 18, 14681-14693, 10.5194/acp-18-14681-2018, 2018b.

469 Liu, P., Li, Y. J., Wang, Y., Gilles, M. K., Zaveri, R. A., Bertram, A. K., and Martin, S. T.: Lability of secondary
470   organic particulate matter, Proceedings of the National Academy of Sciences of the United States of America,
471   113, 12643-12648, 10.1073/pnas.1603138113, 2016.

472 Lv, S., Gong, D., Ding, Y., Lin, Y., Wang, H., Ding, H., Wu, G., He, C., Zhou, L., Liu, S., Ristovski, Z., Chen,
473   D., Shao, M., Zhang, Y., and Wang, B.: Elevated levels of glyoxal and methylglyoxal at a remote mountain site
474   in southern China: Prompt in-situ formation combined with strong regional transport, The Science of the total
475   environment, 672, 869-882, 10.1016/j.scitotenv.2019.04.020, 2019.

Ma, X., Zangmeister, C. D., Gigault, J., Mulholland, G. W., and Zachariah, M. R.: Soot aggregate restructuring during water processing, Journal of Aerosol Science, 66, 209-219, 10.1016/j.jaerosci.2013.08.001, 2013.

Maskey, S., Chong, K. Y., Seo, A., Park, M., Lee, K., and Park, K.: Cloud Condensation Nuclei Activation of Internally Mixed Black Carbon Particles, Aerosol and Air Quality Research, 17, 867-877, 10.4209/aaqr.2016.06.0229, 2017.

Mikhailov, E. F., Vlasenko, S. S., Podgorny, I. A., Ramanathan, V., and Corrigan, C. E.: Optical properties of soot-water drop agglomerates: An experimental study, Journal of Geophysical Research-Atmospheres, 111, D07209, 10.1029/2005jd006389, 2006.

Moffet, R. C., and Prather, K. A.: In-situ measurements of the mixing state and optical properties of soot with implications for radiative forcing estimates, Proceedings of the National Academy of Sciences of the United States of America, 106, 11872-11877, 10.1073/pnas.0900040106, 2009.

Möhler, O., Benz, S., Saathoff, H., Schnaiter, M., Wagner, R., Schneider, J., Walter, S., Ebert, V., and Wagner, S.: The effect of organic coating on the heterogeneous ice nucleation efficiency of mineral dust aerosols, Environmental Research Letters, 3, 025007, 10.1088/1748-9326/3/2/025007, 2008.

Myriokefalitakis, S., Tsigaridis, K., Mihalopoulos, N., Sciare, J., Nenes, A., Kawamura, K., Segers, A., and Kanakidou, M.: In-cloud oxalate formation in the global troposphere: a 3-D modeling study, Atmospheric Chemistry and Physics, 11, 5761-5782, 10.5194/acp-11-5761-2011, 2011.

Ogawa, S., Setoguchi, Y., Kawana, K., Nakayama, T., Ikeda, Y., Sawada, Y., Matsumi, Y., and Mochida, M.: Hygroscopicity of aerosol particles and CCN activity of nearly hydrophobic particles in the urban atmosphere over Japan during summer, Journal of Geophysical Research-Atmospheres, 121, 7215-7234, 10.1002/2015jd024636, 2016.

Oh, C., and Sorensen, C. M.: The effect of overlap between monomers on the determination of fractal cluster morphology, Journal of Colloid and Interface Science, 193, 17-25, 10.1006/jcis.1997.5046, 1997.

Ovadnevaite, J., Zuend, A., Laaksonen, A., Sanchez, K. J., Roberts, G., Ceburnis, D., Decesari, S., Rinaldi, M., Hodas, N., Facchini, M. C., Seinfeld, J. H., and Dowd, C. O.: Surface tension prevails over solute effect in organic-influenced cloud droplet activation, Nature, 546, 637-641, 10.1038/nature22806, 2017.

Pierce, J. R., Leaitch, W. R., Liggio, J., Westervelt, D. M., Wainwright, C. D., Abbatt, J. P. D., Ahlm, L., Al-Basheer, W., Cziczo, D. J., Hayden, K. L., Lee, A. K. Y., Li, S. M., Russell, L. M., Sjostedt, S. J., Strawbridge, K. B., Travis, M., Vlasenko, A., Wentzell, J. J. B., Wiebe, H. A., Wong, J. P. S., and Macdonald, A. M.: Nucleation and condensational growth to CCN sizes during a sustained pristine biogenic SOA event in a forested mountain valley, Atmospheric Chemistry and Physics, 12, 3147-3163, 10.5194/acp-12-3147-2012, 2012.

Qiu, C., Khalizov, A. F., and Zhang, R.: Soot Aging from OH-Initiated Oxidation of Toluene, Environmental Science & Technology, 46, 9464-9472, 10.1021/es301883y, 2012.

Radney, J. G., You, R., Ma, X., Conny, J. M., Zachariah, M. R., Hodges, J. T., and Zangmeister, C. D.: Dependence of Soot Optical Properties on Particle Morphology: Measurements and Model Comparisons, Environmental Science & Technology, 48, 3169-3176, 10.1021/es4041804, 2014.

Raymond, T. M., and Pandis, S. N.: Cloud activation of single-component organic aerosol particles, Journal of Geophysical Research-Atmospheres, 107, D24, 10.1029/2002jd002159, 2002.

Riva, M., Chen, Y., Zhang, Y., Lei, Z., Olson, N. E., Boyer, H. C., Narayan, S., Yee, L. D., Green, H. S., Cui, T., Zhang, Z., Baumann, K., Fort, M., Edgerton, E., Budisulistiorini, S. H., Rose, C. A., Ribeiro, I. O., e Oliveira, R. L., dos Santos, E. O., Machado, C. M. D., Szopa, S., Zhao, Y., Alves, E. G., de Sá, S. S., Hu, W., Knipping, E. M., Shaw, S. L., Duvoisin Junior, S., de Souza, R. A. F., Palm, B. B., Jimenez, J.-L., Glasius, M., Goldstein, A. H., Pye, H. O. T., Gold, A., Turpin, B. J., Vizuete, W., Martin, S. T., Thornton, J. A., Dutcher, C. S., Ault, A. P., and Surratt, J. D.: Increasing Isoprene Epoxydiol-to-Inorganic Sulfate Aerosol Ratio Results in Extensive Conversion of Inorganic Sulfate to Organosulfur Forms: Implications for Aerosol Physicochemical Properties, Environmental Science & Technology, 53, 8682-8694, doi:10.1021/acs.est.9b01019, 2019.

Roth, A., Schneider, J., Klimach, T., Mertes, S., van Pinxteren, D., Herrmann, H., and Borrmann, S.: Aerosol properties, source identification, and cloud processing in orographic clouds measured by single particle mass spectrometry on a central European mountain site during HCCT-2010, Atmospheric Chemistry and Physics, 16, 505-524, 10.5194/acp-16-505-2016, 2016.

Salam, A., Bauer, H., Kassin, K., Ullah, S. M., and Puxbaum, H.: Aerosol chemical characteristics of a mega-city in Southeast Asia (Dhaka-Bangladesh), Atmospheric Environment, 37, 2517-2528, 10.1016/s1352-2310(03)00135-3, 2003.

Scott, C. E., Rap, A., Spracklen, D. V., Forster, P. M., Carslaw, K. S., Mann, G. W., Pringle, K. J., Kivekäs, N., Kulmala, M., Lihavainen, H., and Tunved, P.: The direct and indirect radiative effects of biogenic secondary organic aerosol, Atmospheric Chemistry and Physics, 14, 447-470, 10.5194/acp-14-447-2014, 2014.

Shingler, T., Dey, S., Sorooshian, A., Brechtel, F. J., Wang, Z., Metcalf, A., Coggon, M., Mülmenstäd, J., Russell, L. M., Jonsson, H. H., and Seinfeld, J. H.: Characterisation and airborne deployment of a new counterflow virtual impactor inlet, Atmospheric Measurement Techniques, 5, 1259-1269, 10.5194/amt-5-1259-2012, 2012.

Shiraiwa, M., Zuend, A., Bertram, A. K., and Seinfeld, J. H.: Gas-particle partitioning of atmospheric aerosols: interplay of physical state, non-ideal mixing and morphology, Physical Chemistry Chemical Physics, 15, 11441-11453, 10.1039/c3cp51595h, 2013.

Silva, P. J., Carlin, R. A., and Prather, K. A.: Single particle analysis of suspended soil dust from Southern California, Atmospheric Environment, 34, 1811-1820, 10.1016/s1352-2310(99)00338-6, 2000.

Smith, S., Ward, M., Lin, R., Brydson, R., Dall'Osto, M., and Harrison, R. M.: Comparative study of single particle characterisation by Transmission Electron Microscopy and time-of-flight aerosol mass spectrometry in the London atmosphere, Atmospheric Environment, 62, 400-407, 10.1016/j.atmosenv.2012.08.028, 2012.

Song, M., Marcolli, C., Krieger, U. K., Lienhard, D. M., and Peter, T.: Morphologies of mixed organic/inorganic/aqueous aerosol droplets, Faraday Discussions, 165, 289-316, 10.1039/c3fd00049d, 2013.

Spencer, M. T., and Prather, K. A.: Using ATOFMS to determine OC/EC mass fractions in particles, Aerosol Science and Technology, 40, 585-594, 10.1080/02786820600729138, 2006.

Spracklen, D. V., Jimenez, J. L., Carslaw, K. S., Worsnop, D. R., Evans, M. J., Mann, G. W., Zhang, Q., Canagaratna, M. R., Allan, J., Coe, H., McFiggans, G., Rap, A., and Forster, P.: Aerosol mass spectrometer constraint on the global secondary organic aerosol budget, Atmospheric Chemistry and Physics, 11, 12109-12136, 10.5194/acp-11-12109-2011, 2011.

Topping, D. O., McFiggans, G. B., Kiss, G., Varga, Z., Facchini, M. C., Decesari, S., and Mircea, M.: Surface tensions of multi-component mixed inorganic/organic aqueous systems of atmospheric significance:

measurements, model predictions and importance for cloud activation predictions, Atmospheric Chemistry and Physics, 7, 2371-2398, 10.5194/acp-7-2371-2007, 2007.

Twohy, C. H., and Anderson, J. R.: Droplet nuclei in non-precipitating clouds: composition and size matter, Environmental Research Letters, 3, 045002, 10.1088/1748-9326/3/4/045002, 2008.

Wang, Y., Liu, F., He, C., Bi, L., Cheng, T., Wang, Z., Zhang, H., Zhang, X., Shi, Z., and Li, W.: Fractal Dimensions and Mixing Structures of Soot Particles during Atmospheric Processing, Environmental Science & Technology Letters, 4, 487-493, 10.1021/acs.estlett.7b00418, 2017.

Wu, Y., Cheng, T., Liu, D., Allan, J. D., Zheng, L., and Chen, H.: Light Absorption Enhancement of Black Carbon Aerosol Constrained by Particle Morphology, Environmental Science & Technology, 52, 6912-6919, 10.1021/acs.est.8b00636, 2018.

Wu, Z. J., Poulain, L., Henning, S., Dieckmann, K., Birmili, W., Merkel, M., van Pinxteren, D., Spindler, G., Mueller, K., Stratmann, F., Herrmann, H., and Wiedensohler, A.: Relating particle hygroscopicity and CCN activity to chemical composition during the HCCT-2010 field campaign, Atmospheric Chemistry and Physics, 13, 7983-7996, 10.5194/acp-13-7983-2013, 2013.

Xu, W., Han, T., Du, W., Wang, Q., Chen, C., Zhao, J., Zhang, Y., Li, J., Fu, P., Wang, Z., Worsnop, D. R., and Sun, Y.: Effects of aqueous-phase and photochemical processing on secondary organic aerosol formation and evolution in Beijing, China, Environmental Science & Technology, 51, 762-770, 10.1021/acs.est.6b04498, 2017.

Ye, L., Huang, M., Zhong, B., Wang, X., Tu, Q., Sun, H., Wang, C., Wu, L., and Chang, M.: Wet and dry deposition fluxes of heavy metals in Pearl River Delta Region (China): Characteristics, ecological risk assessment, and source apportionment, Journal of Environmental Sciences-China, 70, 106-123, 10.1016/j.jes.2017.11.019, 2018.

Yu, H., Li, W., Zhang, Y., Tunved, P., Dall'Osto, M., Shen, X., Sun, J., Zhang, X., Zhang, J., and Shi, Z.: Organic coating on sulfate and soot particles during late summer in the Svalbard Archipelago, Atmospheric Chemistry and Physics, 19, 10433-10446, 10.5194/acp-19-10433-2019, 2019.

Yuan, Q., Xu, J., Wang, Y., Zhang, X., Pang, Y., Liu, L., Bi, L., Kang, S., and Li, W.: Mixing State and Fractal Dimension of Soot Particles at a Remote Site in the Southeastern Tibetan Plateau, Environmental Science & Technology, 53, 8227-8234, 10.1021/acs.est.9b01917, 2019.

Zelenyuk, A., Imre, D., Earle, M., Easter, R., Korolev, A., Leaitch, R., Liu, P., Macdonald, A. M., Ovchinnikov, M., and Strapp, W.: In Situ Characterization of Cloud Condensation Nuclei, Interstitial, and Background Particles Using the Single Particle Mass Spectrometer, SPLAT II, Analytical Chemistry, 82, 7943-7951, 10.1021/ac1013892, 2010.

Zhang, G., Lin, Q., Peng, L., Bi, X., Chen, D., Li, M., Li, L., Brechtel, F. J., Chen, J., Yan, W., Wang, X., Peng, P., Sheng, G., and Zhou, Z.: The single-particle mixing state and cloud scavenging of black carbon: a case study at a high-altitude mountain site in southern China, Atmospheric Chemistry and Physics, 17, 14975-14985, 10.5194/acp-17-14975-2017, 2017a.

Zhang, G., Lin, Q., Peng, L., Yang, Y., Fu, Y., Bi, X., Li, M., Chen, D., Chen, J., Cai, Z., Wang, X., Peng, P., Sheng, G., and Zhou, Z.: Insight into the in-cloud formation of oxalate based on in situ measurement by single particle mass spectrometry, Atmospheric Chemistry and Physics, 17, 13891-13901, 10.5194/acp-17-13891-2017, 2017b.

594 Zhang, R., Khalizov, A. F., Pagels, J., Zhang, D., Xue, H., and McMurry, P. H.: Variability in morphology,
595   hygroscopicity, and optical properties of soot aerosols during atmospheric processing, Proceedings of the
596   National Academy of Sciences of the United States of America, 105, 10291-10296, 10.1073/pnas.0804860105,
597   2008.

598 Zhang, Y., Chen, Y., Lambe, A. T., Olson, N. E., Lei, Z., Craig, R. L., Zhang, Z., Gold, A., Onasch, T. B., Jayne,
599   J. T., Worsnop, D. R., Gaston, C. J., Thornton, J. A., Vizuete, W., Ault, A. P., and Surratt, J. D.: Effect of the
600   Aerosol-Phase State on Secondary Organic Aerosol Formation from the Reactive Uptake of Isoprene-Derived
601   Epoxydiols (IEPOX), Environmental Science & Technology Letter, 5, 167-174,
602   doi:10.1021/acs.estlett.8b00044, 2018.

603 Zhang, Y., Chen, Y., Lei, Z., Olson, N. E., Riva, M., Koss, A. R., Zhang, Z., Gold, A., Jayne, J. T., Worsnop, D.
604   R., Onasch, T. B., Kroll, J. H., Turpin, B. J., Ault, A. P., and Surratt, J. D.: Joint Impacts of Acidity and Viscosity
605   on the Formation of Secondary Organic Aerosol from Isoprene Epoxydiols (IEPOX) in Phase Separated
606   Particles, ACS Earth Space Chem., 3, 2646-2658, doi:10.1021/acsearthspacechem.9b00209, 2019.

607 Zhang, Y., Yuan, Q., Huang, D., Kong, S., Zhang, J., Wang, X., Lu, C., Shi, Z., Zhang, X., Sun, Y., Wang, Z.,
608   Shao, L., Zhu, J., and Li, W.: Direct Observations of Fine Primary Particles From Residential Coal Burning:
609   Insights Into Their Morphology, Composition, and Hygroscopicity, Journal of Geophysical Research-
610   Atmospheres, 123, 12964-12979, 10.1029/2018jd028988, 2018.

611 Zhu, J., Penner, J. E., Lin, G., Zhou, C., Xu, L., and Zhuang, B.: Mechanism of SOA formation determines
612   magnitude of radiative effects, Proceedings of the National Academy of Sciences of the United States of
613   America, 114, 12685-12690, 10.1073/pnas.1712273114, 2017.

614 **Table 1. The information of cloud events and samples, including starting and ending time of each cloud event, the number and type of analyzed particles, the mean value**
615 **of visibility and number concentration of RES or INT during sampling time.**
616

Cloud event	Starting Time*	Ending Time*	Particles	Type	Visibility/m	Number Concentration/cm^{-3}
Cloud #1	2017/5/20 18:19	2017/5/21 8:34	190	RES	66	195
Cloud #2	2017/5/23 20:35	2017/5/25 6:35	161	INT	50	99
			162	RES	88	299
Cloud #3	2017/6/8 18:30	2017/6/10 17:30	132	INT	44	996
			135	RES	33	111

617 * The time is the local time and that is Chinese Standard Time, UTC+8.

618   **Table 2. The average value of O/C ratio of OM-containing particles with thinly coated and core-shell mixing structures.**

619

Type	thinly coated	core-shell
RES	0.11	0.23
INT	0.08	0.06

620

621
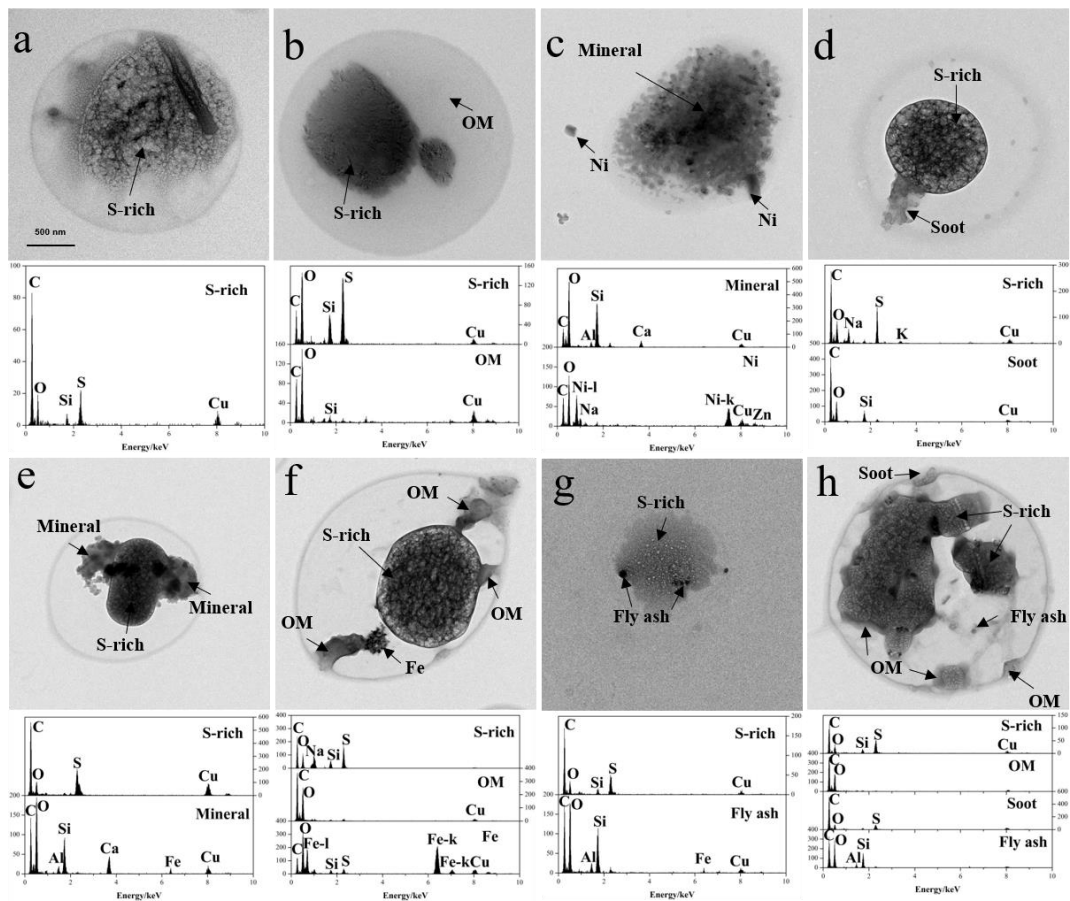
Figure 1. TEM images and EDS spectra of individual RES and INT particles with different particle types: (a) S-rich; (b) S-OM; (c) refractory; (d) aged soot; (e) aged mineral; (f) aged metal; (g) aged fly ash; (h) aged mixture.

625
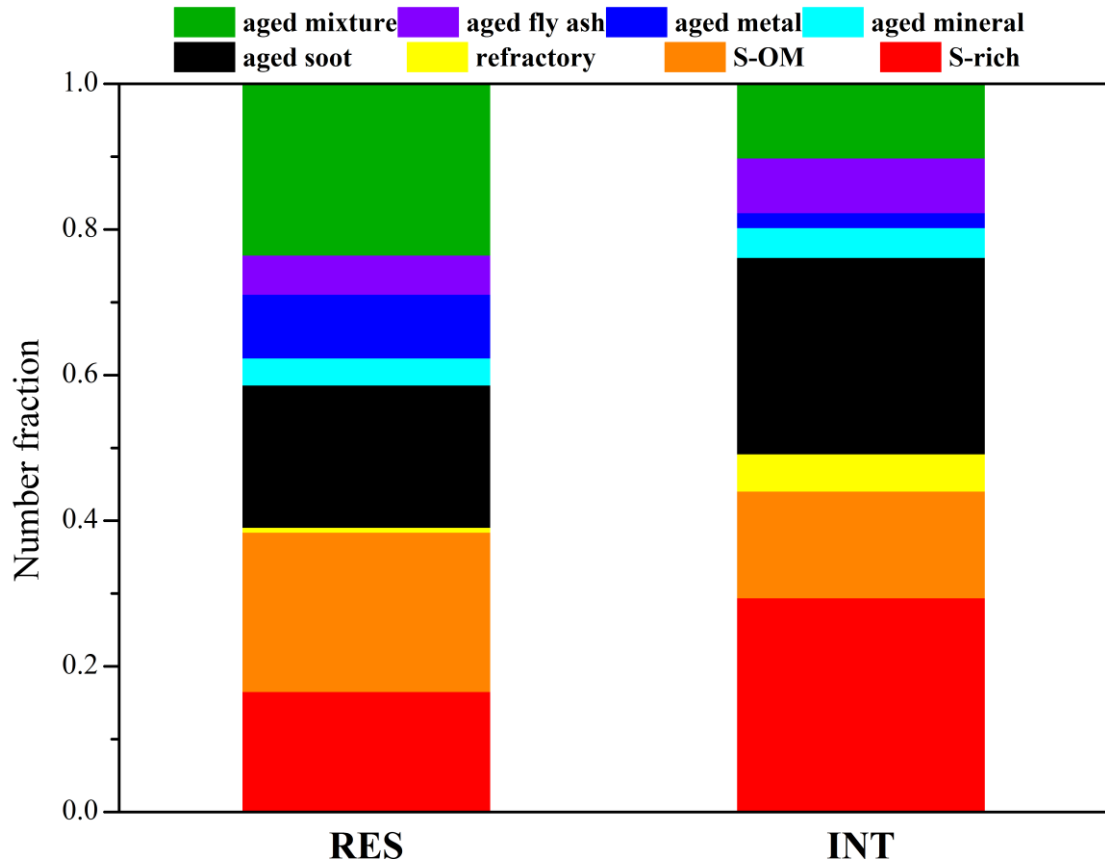
Figure 2. Number fractions of different particle types in the RES and INT of cloud event #2 and #3 measured

627 by TEM/EDS.

Cloud #1   Cloud #2   Cloud #3
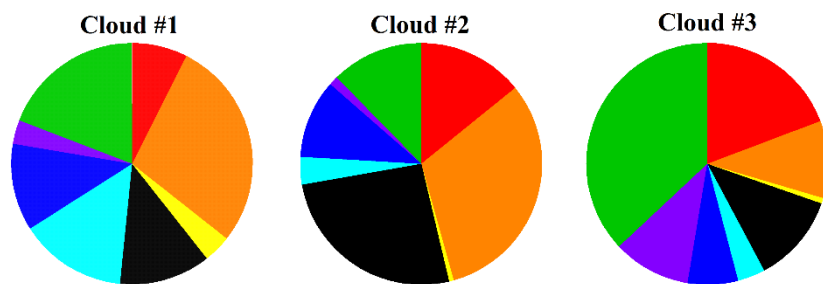
■ S-rich ■ S-OM ■ refractory ■ aged soot ■ aged mineral ■ aged metal ■ aged fly ash ■ aged mixture

628

629

630

631

632
633
634
635
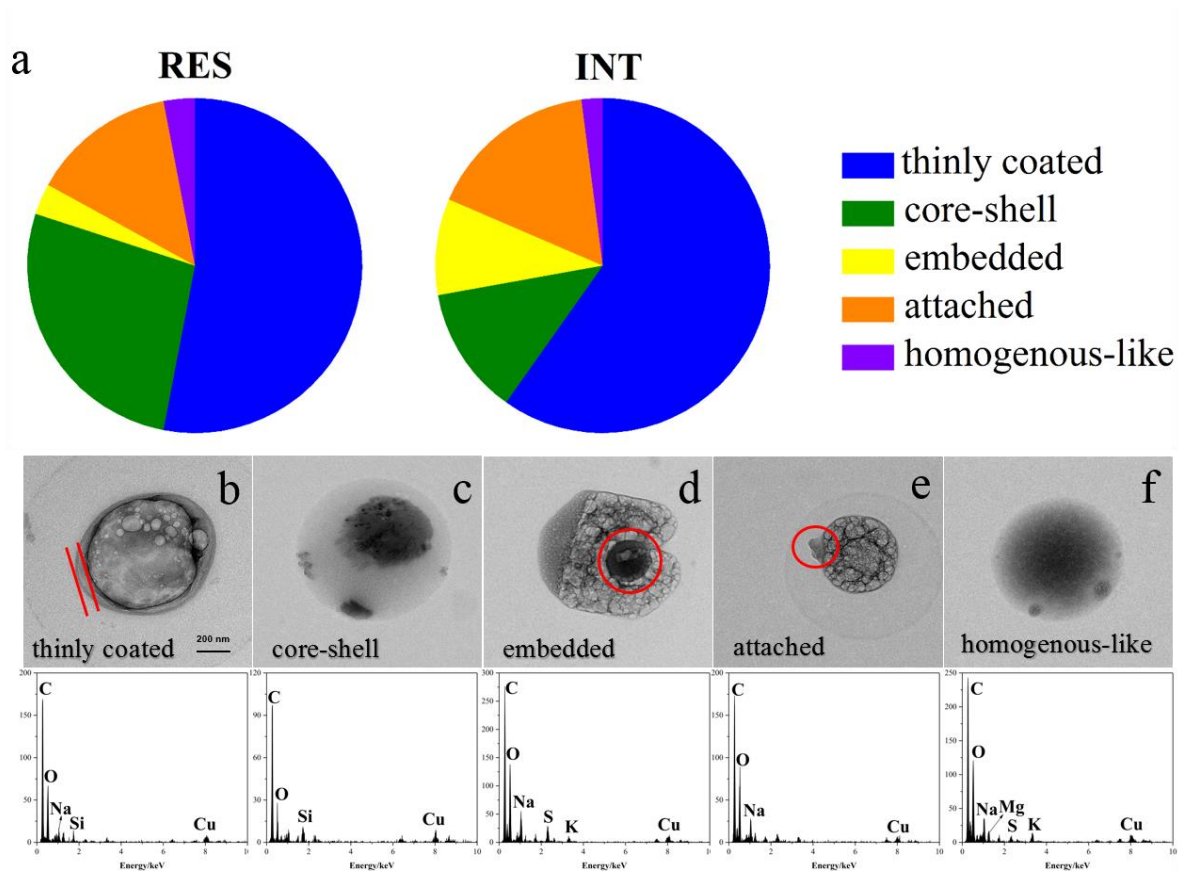
Figure 5. Number fractions of OM-containing particles with different mixing structures in the RES and INT (a) and typical TEM images and corresponding EDS spectra of OM: thinly coated (b); core-shell (c); embedded (d); attached (e); homogenous-like (f) during cloud event #2 and #3.

RES $D_f = 1.82 \pm 0.12$

INT $D_f = 2.11 \pm 0.09$

$N = 3.50(2R_g/d_p)^{1.82}$ $R^2 = 0.74$

$N = 2.72(2R_g/d_p)^{2.11}$ $R^2 = 0.86$
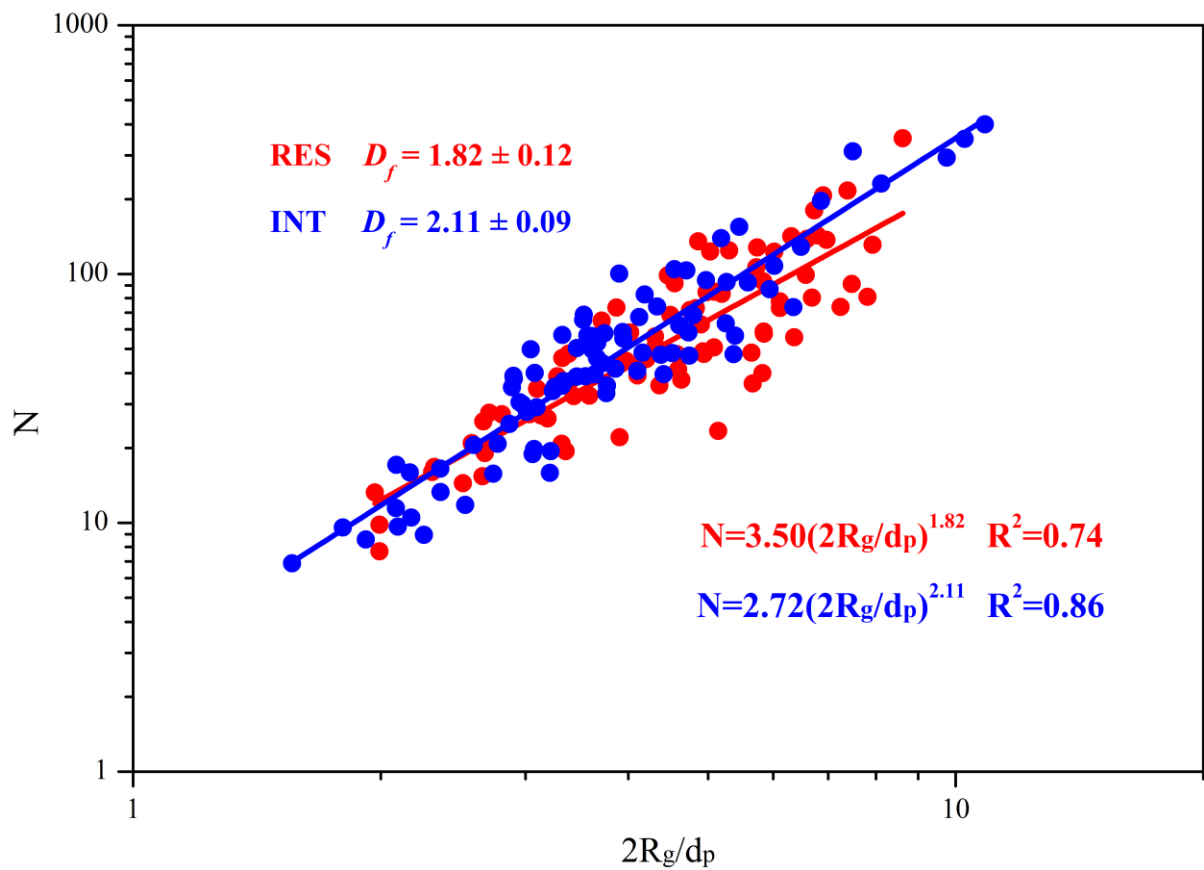
640

641 **Figure 6. Fractal dimensions of soot in the RES and INT during cloud event #2 and #3.**

1 *Supplement of*

Impact of in-cloud aqueous processes on the chemical compositions and morphology of individual atmospheric aerosols

5 **Yuzhen Fu et al.**

6 *Correspondence to*: Guohua Zhang (zhanggh@gig.ac.cn) and Xinhui Bi (bixh@gig.ac.cn)

1 Air mass backward trajectories and meteorology conditions

The backward trajectory and the height (above sea level) of air masses during sampling were calculated by the Hybrid Single Particle Lagrangian Integrated Trajectory (HYSPLIT) model (http://ready.arl.noaa.gov). During three cloud events, the sampling site was greatly influenced by air masses from Southeast Asia, northern China and the South China Sea. Compared with the cloud event #1, the air masses of cloud event #2 and #3 passed through a relatively low path on the way to the sampling site. Thus, the air masses of cloud event #2 and #3 were affected more by the ground anthropogenic emissions. The ambient temperature at the sampling station varied from 12.1 to 18.6 °C during three cloud events, which means the generation of liquid cloud droplets. All samples were collected during the stable period of cloud events, when the mass concentration of $PM_{2.5}$ was less than 5 μg m^{-3} and visibility was less than 100 m. The concentrations of $PM_{2.5}$ during cloud event #1 were lower than those during cloud event #2 and #3. Consistently, the mean concentrations of O_3, SO_2 and NO_X were higher in the cloud event #2 and #3 (Table S1).

2 The size distribution of RES and INT

In this study, a $PM_{2.5}$ cyclone inlet and a GCVI (ground-based counterflow virtual impactor) inlet were used to collect INT and RES, which is similar to Cozic et al. (2007). Additionally, the particle size in this study is ECD (equivalent circle diameter) obtained from TEM images, which is larger than ESD (equivalent spherical diameter). Liu et al. (2018) showed that the ECD of individual dry particles on the substrate is 0.4952 times that of the ESD.

The size distribution data shows a higher median diameter of RES (1.20 μm) than INT (0.63 μm) (Figure S2), which are higher than those (0.8 and 0.45 μm, respectively) at Mount Tai in northern China (Li et al., 2011). This could be due to that Mount Tai is located in an industrial area, whereas our site represents a background region mainly influenced by long-range transport. Additionally, the formation of secondary compounds during cloud events increase the size of RES (Zhang et al., 2017).

The size distribution of different particle types revealed that S-rich and aged soot particles were predominant in smaller size segments, and aged mixture particles in larger size segments (Figure S8). Likewise, the size-resolved number fractions of different particle types from the results of the SPAMS

3 Identification of several types of particles within RES and INT measured by the SPAMS

All particles with bipolar mass spectra and the size range of d_{va} 0.1–1.9 µm were classified several clusters by an adaptive resonance theory neural network (ART-2a) with a learning rate of 0.05, a vigilance factor of 0.8 and 20 iterations, and merged similar clusters manually. Ten characteristic particle types (Figure S1) were obtained including BC (black carbon)-containing, OC (organic carbon), HMOC (highly molecular organic carbon), Dust, K-rich, Metal, Na-K, Amines, SS (sea salt) and Others. BC-containing particles are characterized by elemental carbon cluster ions (m/z $12C^{\pm}$, $24C_2^{\pm}$, $36C_3^{\pm}$, $48C_4^{\pm}$, …). OC particles mainly contain fragment ions of organics (m/z $27C_2H_3^+$, $37C_3H^+$, $43C_2H_3O^+$, -$26CN^-$, …). The mass spectra of HMOC particles show the presence of peaks of OC particles and some other organic peaks (such as m/z $77C_6H_5^+$, $91C_7H_7^+$). Furthermore, HMOC particles are distinguished from OC particles by marked ion fragments detected in range of $m/z > 100$. Dust particles present significant ions at m/z $27Al^+$, $40Ca^+$ and $56CaO^+/Fe^+$. K-rich particles are identified according to the strong signal at m/z $39K^+$ only in positive mass spectra. Metal particles show the presence of metal ion peaks (such as Fe^+ (m/z 54 and 56), Mn^+ (m/z 55), Pb^+ (m/z 206, 207 and 208)) in positive mass spectra. Na-K particles are characterized by peaks at m/z $23Na^+$, $39K^+$, and less intense peaks at m/z -$46NO_2^-$, -$62NO_3^-$, -$97HSO_4^-$. The mass spectra of amines particles contain ions signals at m/z $59N(CH_3)_3^+$, $86C_5H_{12}N^+$, $101C_6H_{15}N^+$. SS particles are mainly composed of ions peaks at m/z $23Na^+$, $46Na_2^+$, $62Na_2O^+$, $63Na_2OH^+$ and $81Na_2Cl^+$. Most particles are observed to internally mixed with sulfate and nitrate (m/z -46, -62, -97). Particles with unconspicuous mass spectrum characteristics are named others. Specific classification criteria were described in detail elsewhere (Zhang et al., 2015).
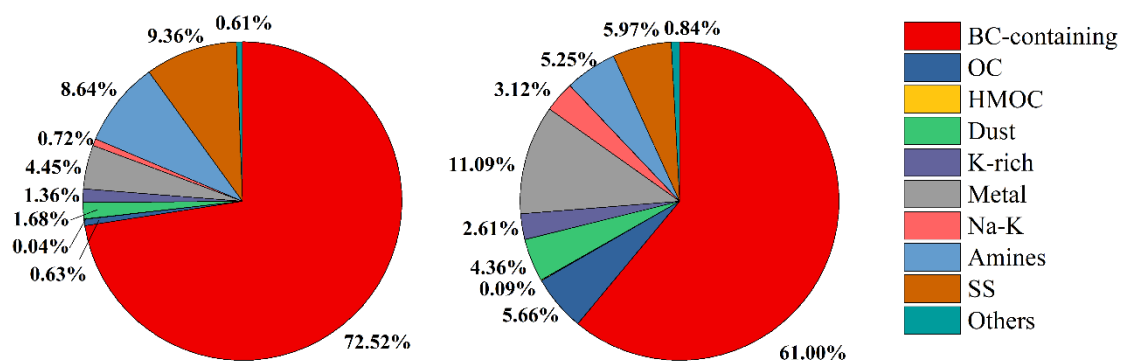
57
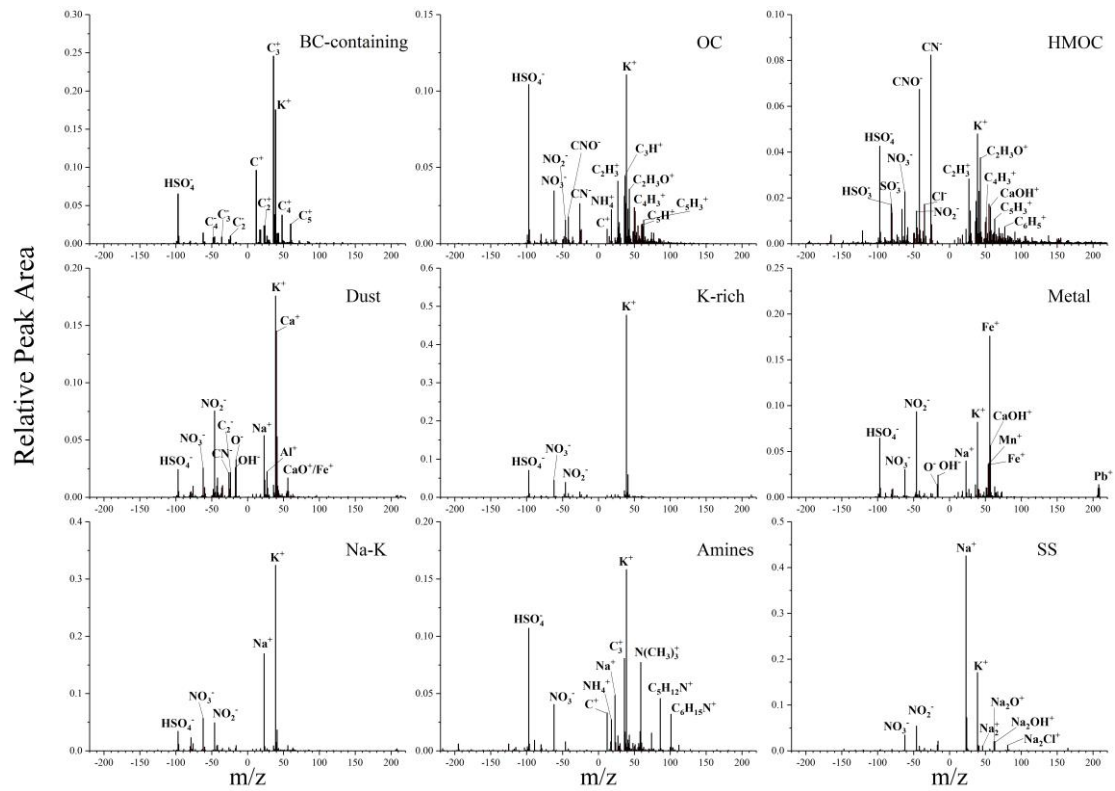
Figure S1. Average positive and negative mass spectra of main nine types particles (BC-containing, OC, HMOC, Dust, K-rich, Metal, Na-K, Amines, SS) measured by SPAMS.
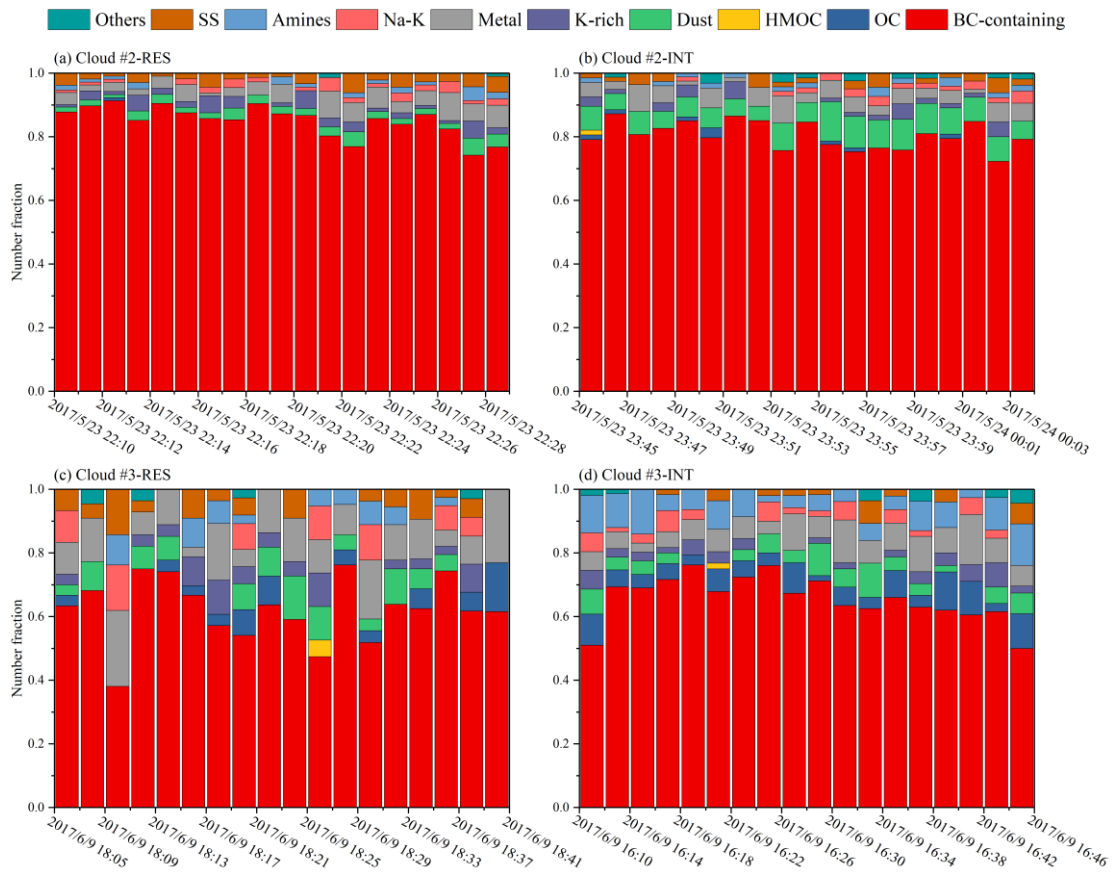
(a) Cloud #2-RES

(b) Cloud #3-RES

9.36%   0.61%
8.64%
0.72%
4.45%
1.36%
1.68%
0.04%
0.63%
72.52%

5.97% 0.84%
5.25%
3.12%
11.09%
2.61%
4.36%
0.09%
5.66%
61.00%

BC-containing
OC
HMOC
Dust
K-rich
Metal
Na-K
Amines
SS
Others

60

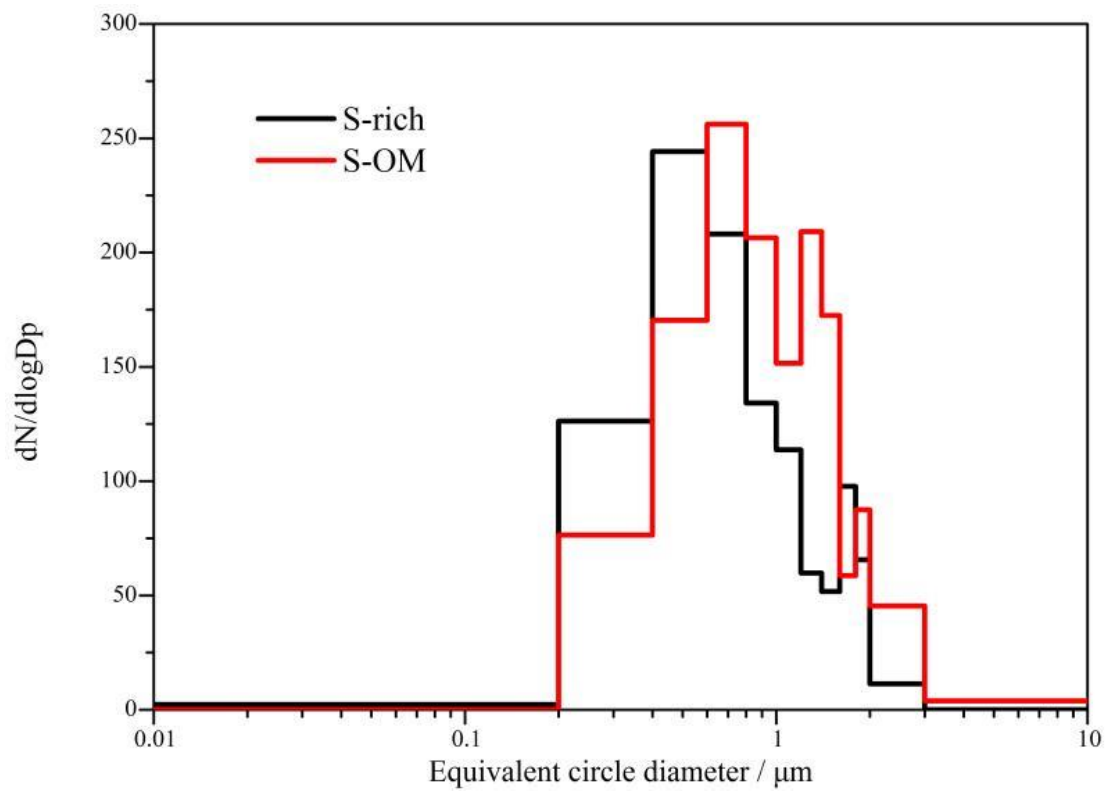61   **Figure S2. The chemical composition of RES during cloud event #2 and #3 measured by SPAMS.**

Figure S3. Time series of chemical composition of RES and INT during sampling periods of cloud event #2 and #3 measured by SPAMS.
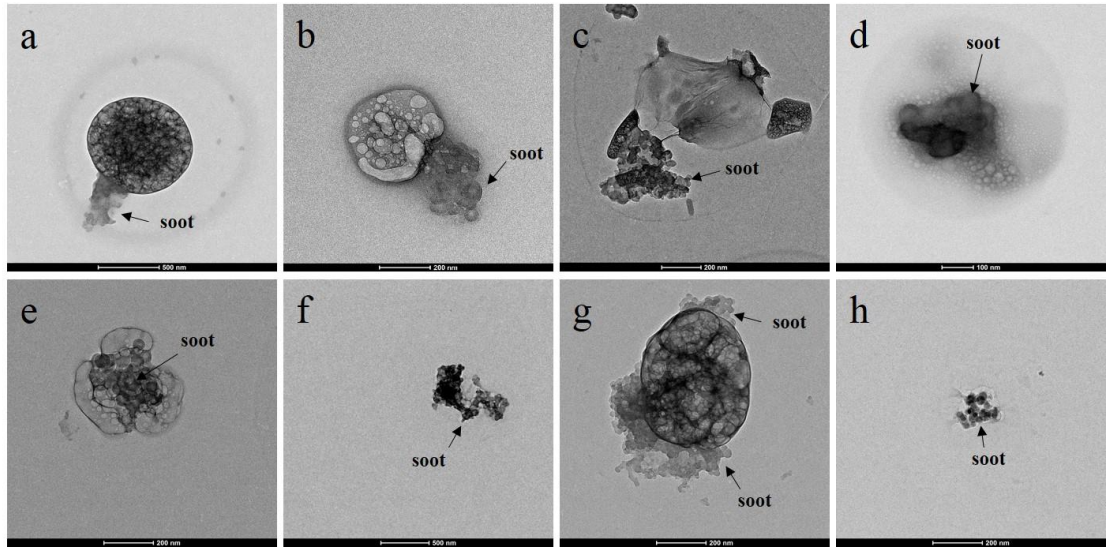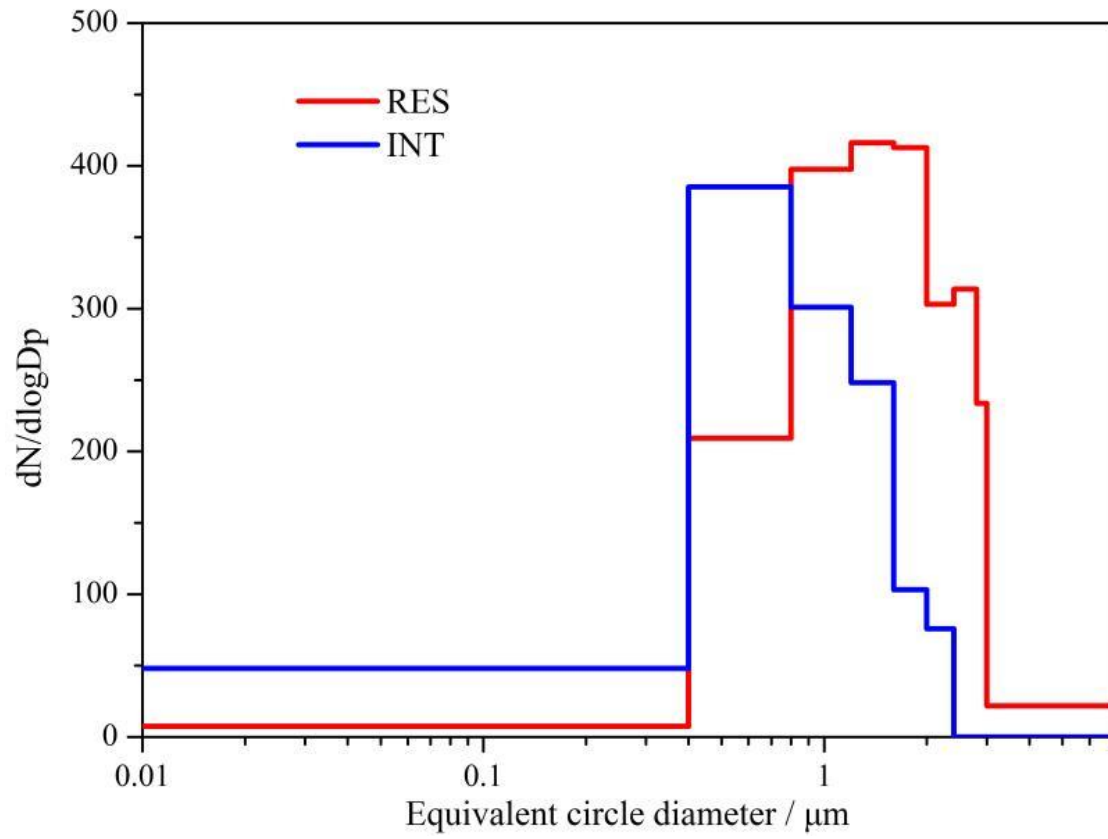
65

66 **Figure S4. Typical TEM images of soot particles in the RES (a-d) and INT (e-h).**

67

**Figure S5. The size distribution of S-rich and S-OM particles. There are few S-rich particles with the size of**

less than 0.2 µm, and the median size are 0.56 µm and 0.76 µm for S-rich and S-OM particles, respectively.

70

Figure S6. Size distribution of RES and INT during cloud event #2 and #3. There are more INT particles

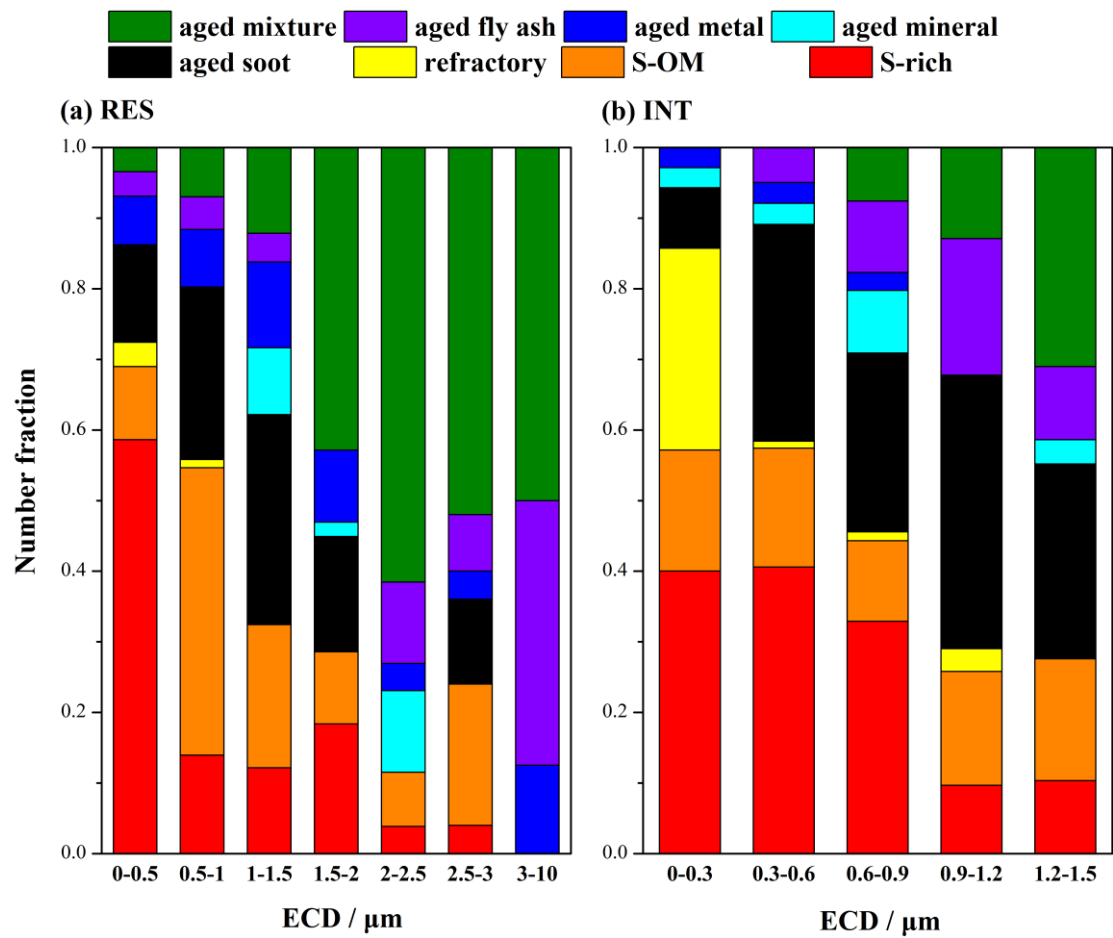when the size is less than 0.8 μm, and more RES particles when the size is larger than 0.8 μm.

73
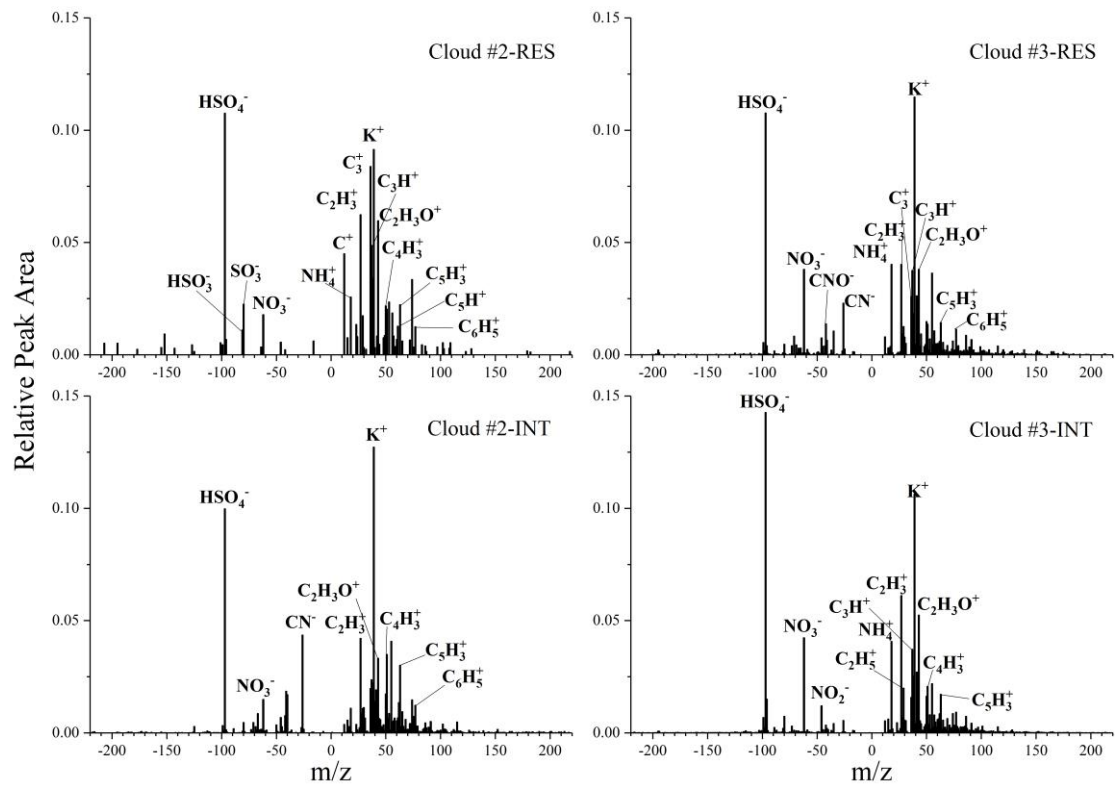
Figure S7. Average positive and negative mass spectra of OM particles (OC and HMOC) of RES and INT

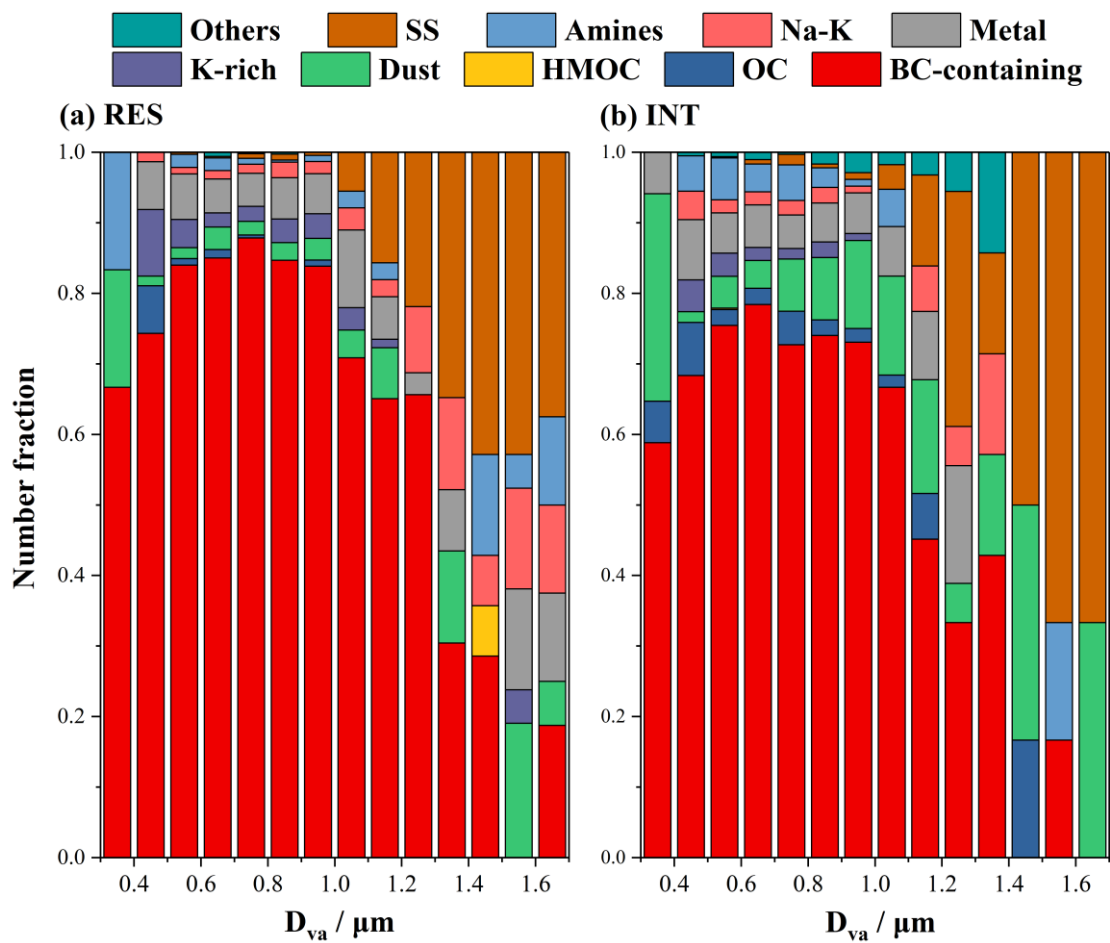74

particles during cloud event #2 and #3 measured by SPAMS.

75

76

Figure S8. Size-resolved number fraction distributions of RES and INT by TEM/EDS.

Figure S9. Size-resolved number fraction distributions of RES and INT by SPAMS.

80   **Table S1.** The concentration of NO_X, SO_2, O_3, PM_{10} and $PM_{2.5}$ during three cloud events.

81

cloud event	NO_X (ppb)	SO_2 (ppb)	O_3 (ppb)	PM_{10} ($\mu g\ m^{-3}$)	$PM_{2.5}$ ($\mu g\ m^{-3}$)
#1	2.6	0.4	30.5	3.6	1.1
#2	3.5	1.2	39.1	4.8	1.9
#3	4.3	0.6	34.4	11.4	4.7

82

83   **Table S2.** The ratios of relative peak area between organics (m/z 27, 29, 37, 43, 50, 51, 61, 63) and sulfate

84   (m/z -97) of OM particles (OC and HMOC) during in-cloud (RES and INT) and pre-cloud (Ambient)

85   periods.

86

87

	RES	INT	Ambient
Organics/Sulfates	1.676	1.566	1.594

88   **Table S3.** Morphological descriptors of soot particles within RES and INT.

89

parameters	A_p	d_p	L_{max}	N	D_f	k_g
RES	1658(175)	43(2)	255(12)	66(8)	1.82(0.12)	3.5(0.08)
INT	1842(133)	46(2)	316(16)	68(6)	2.11(0.09)	2.72(0.05)

90   A_p, mean projected area of the monomer; d_p, monomer diameter; L_{max}, maximum length of soot

91   aggregates; N, number of monomers in a soot aggregate; D_f, mass fractal dimension; k_g, structural

92   coefficient. In parentheses are the standard error of A_p, d_p, L_{max}, N, D_f and k_g.

93   **Table S4.** Overlap (δ), constant (k_a) and empirical exponent (α).

94

parameters	δ	k_a	α
RES	1.54	1.52	1.13
INT	1.4	1.44	1.11

95

96 **References**

97 Cozic, J., Verheggen, B., Mertes, S., Connolly, P., Bower, K., Petzold, A., Baltensperger, U., and

98   Weingartner, E.: Scavenging of black carbon in mixed phase clouds at the high alpine site Jungfraujoch,

99   Atmospheric Chemistry and Physics, 7, 1797-1807, 10.5194/acp-7-1797-2007, 2007.

100 Liu, L., Zhang, J., Xu, L., Yuan, Q., Huang, D., Chen, J., Shi, Z., Sun, Y., Fu, P., Wang, Z., Zhang, D.,

101   and Li, W.: Cloud scavenging of anthropogenic refractory particles at a mountain site in North China,

102   Atmospheric Chemistry and Physics, 18, 14681-14693, 10.5194/acp-18-14681-2018, 2018.

103 Li, W., Li, P., Sun, G., Zhou, S., Yuan, Q., and Wang, W.: Cloud residues and interstitial aerosols from

104   non-precipitating clouds over an industrial and urban area in northern China, Atmospheric

105   Environment, 45, 2488-2495, 10.1016/j.atmosenv.2011.02.044, 2011.

106 Zhang, G., Han, B., Bi, X., Dai, S., Huang, W., Chen, D., Wang, X., Sheng, G., Fu, J., and Zhou, Z.:

107   Characteristics of individual particles in the atmosphere of Guangzhou by single particle mass

108   spectrometry, Atmospheric Research, 153, 286-295, 10.1016/j.atmosres.2014.08.016, 2015.

109 Zhang, G., Lin, Q., Peng, L., Bi, X., Chen, D., Li, M., Li, L., Brechtel, F. J., Chen, J., Yan, W., Wang, X.,

110   Peng, P., Sheng, G., and Zhou, Z.: The single-particle mixing state and cloud scavenging of black

111   carbon: a case study at a high-altitude mountain site in southern China, Atmospheric Chemistry and

112   Physics, 17, 14975-14985, 10.5194/acp-17-14975-2017, 2017.